

# Experimental Study of Flow Separation Control on an Airfoil by Suction and Injection

By

Md. Farhad Hossain



A project report submitted to the Department of the Mechanical Engineering in  
partial fulfillment of the requirements for the degree of Master of Science in  
Mechanical Engineering



Khulna University of Engineering & Technology  
Khulna 9203, Bangladesh  
May, 2010

## Declaration

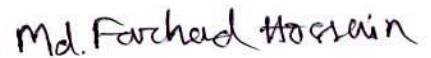
This is to certify that the project work entitled " *Experimental Study of Flow Separation Control on an Airfoil by Suction and injection*" carried by Md. Farhad Hossain in the Department of Mechanical Engineering, Khulna University of Engineering & Technology, Bangladesh. The above research work or any-part of the work has not been submitted anywhere for the award of any degree or diploma.

  
\_\_\_\_\_

Signature of the Supervisor

Name: Dr. Mohammad Mashud

Designation: Associate Professor

  
\_\_\_\_\_

Signature of the Candidate



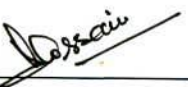

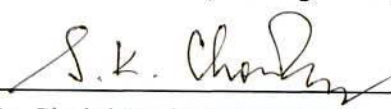
Name: Md. Farhad Hossain

Roll No.: 0805552

## Approval

This is to certify that the project work submitted by Md. Farhad Hossain entitled "*Experimental Study of Flow Separation Control on an Airfoil by Suction and Injection*" has been approved by the Board of Examiners for the partial fulfillment of the requirements for the degree of Master of Science in Mechanical Engineering in the Department of Mechanical Engineering, Khulna University of Engineering & Technology, Bangladesh in May'2010.

### BOARD OF EXAMINERS

1.   
Dr. Mohammad Mashud  
Associate Professor, Department of Mechanical Engineering  
Khulna University of Engineering & Technology  
Chairman  
(Supervisor)
2.   
Professor Dr. Mihir Ranjan Halder  
Head  
Department of Mechanical Engineering  
Khulna University of Engineering & Technology  
Member
3.   
Dr. Khandkar Aftab Hossain  
Professor, Department of Mechanical Engineering  
Khulna University of Engineering & Technology  
Member
4.   
Dr. A. N. M. Mizanur Rahman  
Professor, Department of Mechanical Engineering  
Khulna University of Engineering & Technology  
Member
5.   
Dr. Sirajul Karim Choudhury  
Professor, Department of Mechanical Engineering  
Rajshahi University of Engineering & Technology  
Member (External)

## ACKNOWLEDGEMENTS

The author expresses his most sincere thanks to his project supervisor Dr. Mohammad Mashud, Associate Professor, Department of Mechanical Engineering of Khulna University of Engineering & Technology (KUET). Without his all-around help, input, and support throughout the entire project, this thesis could not have been completed. The advice and trust of Prof. Dr. Mihir Ranjan Halder (Department of Mechanical Engineering of Khulna University of Engineering & Technology, KUET) is always welcome. The patience and the help that he cares to give are appreciated. Special thanks to Prof. Dr. Khandakar Aftab Hossain and Prof. Dr. A. N. M. Mizanur Rahman (Department of Mechanical Engineering of Khulna University of Engineering & Technology, KUET) for being members of the Examination Committee.

Mrs. Rekha Khatun, my mother, the rest of my family, especially my father, brother, and sister, my friends is thanked for their continued support. Also, I want to thank Mr. Harun, A.T.O. of Machine Shop for constructing the apparatus and Mr. Rezaul Karim A.T.O. Fluid Mechanics Lab for their help during experiment. Mr. Mahfuz Sarwar, Lecturer Department of Mechanical Engineering of Khulna University of Engineering & Technology, is needed to be recognized for always being helpful and at hand whenever work has to be done.

Author

## ABSTRACT

In this research a new concept of flow separation control mechanism has been introduced to improve the aerodynamic characteristics of an airfoil. Control of flow separation over an airfoil which experiences a laminar separation bubble for a low Reynolds number is experimentally simulated under the effects of suction and injection. The suction and injection control mechanism appears to be suppression of the separation bubble and reduction of the upper surface pressure to increase the lift and decrease the drag. To perform the experiment of NACA 2415 airfoil profile has been chosen to make wing model. The wing model with control mechanism has been tested in a sub-sonic wind tunnel. The experiments are performed with different angle of attack and different suction-injection frequency. The experimental results show that the flow separation control is possible by the proposed mechanism and benefits can be achieved by suction and injection. The wing performance is significantly improved due to control of flow separation by suction and injection. It has also been found that the lift increases about 14% and drag reduces about 23% at the angle of attack 8 degree.

# Contents

	<b>Page</b>
Title Page	i
Declaration	ii
Approval	iii
Acknowledgements	iv
Abstract	v
Contents	vi
List of Tables	ix
List of Figures	x
Nomenclature	xii

## CHAPTER I

Introduction	
1.1 General	1
1.2 Objectives	3
1.3 Background	3
1.3.1 Motion of Solid Wall	3
1.3.2 Slit Suction	4
1.3.3 Tangential Blowing and Suction	4
1.3.4 Continuous Suction and Blowing	4
1.3.5 Using vortex generate jets	5
1.3.6 Pulse jet	5
1.3.7 Acoustically Active Surfaces	6
1.3.8 Synthetic jet	6

## CHAPTER II

Literature Review	
2.1 Historical Background	7
2.2 Flow Phenomena	8
2.2.1 Laminar flow	11
2.2.2 Transient flow	11

	<b>Page</b>
2.2.3 Turbulent flow	12
2.2.4 Compressible Flow	13
2.2.5 Incompressible Flow	13
2.2.6 Couette Flow	14
2.2.7 Secondary Flow	14
2.3 Unifying Principles	14
2.3.1 Active Control	18
2.3.2 Passive Control	18
2.3.3 Reactive Control	19
2.3.4 Reactive Feedback Control	20
2.4 Wall-Bounded and Free-Shear Flows	21
2.4.1 Inviscid and Viscous Instabilities	22
2.4.2 Regimes of Reynolds and Mach Numbers	22
2.4.3 Convective and Absolute Instabilities	24
2.4.4 Classical Control Tools	25
2.5 Conclusions	26



### **CHAPTER III**

#### Methodology

3.1 Flow separation control mechanism	28
---------------------------------------	----

### **CHAPTER IV**

#### Experimental Setup and Procedure

4.1 Introduction	30
4.2 Wind Tunnel	30
4.3 Construction of Model (wing)	31
4.4 Experimental Setup	33
4.4.1 Pressure Measurement	36

## **CHAPTER V**

	<b>Page</b>
<b>Results and Discussion</b>	
5.1 Motivation	37
5.2 Results and Discussion	39
5.2.1 Pressure Distribution	39

## **CHAPTER VI**

<b>Conclusions</b>	
6.0 Conclusions	55
<b>Recommendations</b>	56
<b>Reference</b>	57
<b>Appendix A</b>	60
<b>Appendix B</b>	71



## List of Tables

<b>Table No.</b>	<b>Description</b>	<b>Page</b>
Table 5.1	Lift Co-efficient $C_l$ for different frequencies	52
Table 5.2	Drag Co-efficient $C_d$ for different frequencies	53

## List of Figure

<b>Figure No.</b>	<b>Description</b>	<b>Page</b>
Figure 2.1	Classification of Flow Control Strategies	16
Figure 2.2 (a)	Different Control Loops for Active Flow Control	17
Figure 2.2 (b)	Different Control Loops for Active Flow Control	17
Figure 2.2 (c)	Different Control Loops for Active Flow Control	17
Figure 4.2	Subsonic Wind Tunnels Schematic	31
Figure 4.3(a)	Construction of Model NACA 2415 with four slots	32
Figure 4.3(b)	Construction of Model NACA 2415 with four holes	33
Figure 4.4(a)	Experimental set up in schematic drawing	34
Figure 4.4(b)	Experimental set up of model in wing tunnel	34
Figure 4.4(c)	Experimental set up model with single piston mechanism	35
Figure 4.4(d)	Airfoil geometry of NACA 2415	35
Figure 4.4(A):	Calibration Curve of Digital Manometer	36
Figure 5.1(a)	The flow around a flat plate placed in uniform flow.	37
Figure 5.1(b)	The flow around a symmetric airfoil placed in uniform flow	38
Figure 5.1(c)	The flow around a circular arc airfoil placed in uniform flow	38
Figure 5.1(d)	The flow around the General Joukowski Airfoil placed in uniform flow	38
Figure 5.2(a)	Pressure coefficient distribution along the cord at $\alpha = 0$ degree	41
Figure 5.2(b)	Pressure coefficient distribution along the cord at $\alpha = 2$ degree	41
Figure 5.2(c)	Pressure coefficient distribution along the cord at $\alpha = 4$ degree	42
Figure 5.2(d)	Pressure coefficient distribution along the cord at $\alpha = 6$ degree	42
Figure 5.2(e)	Pressure coefficient distribution along the cord at $\alpha = 8$ degree	43
Figure 5.2(f)	Pressure coefficient distribution along the cord at $\alpha = 10$ degree	44
Figure 5.2(g)	Pressure coefficient distribution along the cord at $\alpha = 12$ degree	45
Figure 5.2(h)	Pressure coefficient distribution along the cord at $\alpha = 14$ degree	46
Figure 5.2(i)	Pressure coefficient distribution along the cord at $\alpha = 20$ degree	46

<b>Figure No.</b>	<b>Description</b>	<b>Page</b>
Figure 5.2(A)	Comparison of the experimental pressure distribution (No jet) over the NACA 2415 aerofoil and the numerical pressure distributions by suction	47
Figure 5.2(B)	Comparison of the experimental pressure distribution (No jet) over the NACA 2415 aerofoil and the numerical pressure distributions by injection	47
Figure 5.2(j)	Lift Coefficient $C_l$ vs $\alpha$	48
Figure 5.2(k)	Drag Coefficient $C_d$ vs $\alpha$	49
Figure 5.2(l)	Lift and Drag ratio vs $\alpha$	50
Figure 5.2(m)	Coefficient of Lift vs Drag curve	51

## Nomenclature

$C_l$	= Lift Coefficient
$C_d$	= Drag Coefficient
$C_p$	= Pressure Coefficient
$L$	= Lift
$D$	= Drag
$U_\infty$	= Free Stream Velocity
$C$	= Chord Length
$\alpha$	= Angle of Attack
$Re$	= Reynolds Number
$f_c$	= Excitation Frequency
$F$	= Reduced Frequency
$x/c$	= Normalized Stream wise Location
$X_R$	= Distance from the Slot to Flow Reattachment
$\rho_\infty$	= Free stream density
$q_\infty$	= Dynamic pressure
$\alpha$	= Angle of Attack
$\mu$	= Dynamic viscosity
$\nu$	= Kinematic Viscosity
$M_a$	= Mach number
$C_{pu}$	= Coefficient of Pressure (Upper Surface)
$C_{pL}$	= Coefficient of Pressure (Lower Surface)

# CHAPTER I

## INTRODUCTION

### 1.1 General

The ability to manipulate a flow field to effect a desired change is of immense practical importance. As a scientific discipline and as a technological curiosity, flow control is perhaps more hotly pursued by scientists and engineers than any other area in fluid mechanics, especially in aerodynamics, with the purpose of reducing total energy consumption by increasing lift force and decreasing drag force of airfoils. The concept of flow separation control is not new, with boundary layer blowing or suction to delay flow separation is known since Prandtl [1]. Flow control involves passive or active devices; passive control devices are those, which are not energy consumptive. They mainly affect the flow by the geometry of the airfoil. In contrast, active control devices use energy such as surface suction or injection, to effect a beneficial change in wall-bounded or free-shear flows. Whether the task is to delay/advance transition, to suppress/enhance turbulence or to prevent/provoke separation, useful end results include drag reduction, lift enhancement, mixing augmentation and flow-induced noise suppression.

Drag reduction is one of the basic scientific and technological issues for large transport airplane development. Within the airplane's cruising drag, friction drag is an important component, especially for subsonic airplanes, with surface friction drag accounting for almost 50% of the total drag [2]. Therefore, friction drag reduction becomes a significant topic in the current airplane drag reduction design. Furthermore, as friction drag at the turbulent boundary layer is far greater than that at the laminar boundary layer, the basic idea of friction drag reduction is focused on delaying the occurrence of transition, expanding the range of laminar flow at the object surface, and reducing friction drag at the turbulent boundary layer. Among various drag-reduction control techniques, laminar flow control is a very effective method for friction drag reduction. It can stabilize an unstable boundary layer by inhibiting the development and amplification of various unstable disturbance waves inside the boundary layers through control measures, and accordingly, it delays the transition from laminar flow to turbulent flow at the boundary layer [2]. Transition-delaying compliant coatings were rationally optimized using computational fluid dynamics [3]. By controlling the flow,

the fuel burned might be decreased almost 30 percent as reported by Braslow [4]. As a result, the pollutant emissions are reduced. In addition, lower fuel consumption will reduce the operating costs of commercial airplanes at least 8% [4]. In active laminar flow control it is required to keep the flow laminar on the surface. Flow control is a technology that offers the potential for improvements in aircraft fuel consumption. This broad area of research remains of great interest for its numerous potential benefits for both the military and civilian sectors [2].

The simplest active flow control system is surface suction and injection. Suction and injection of a secondary airflow can have significant effects on the flow field. They affect particularly the shape of the velocity profile near the wall and change the boundary layer shape. An inflectional velocity profile can be produced by injection, adverse pressure-gradient or higher wall viscosity. Such profile is more prone to transition and to separation and is associated with lower, even negative, skin friction [5].

Taking the previously mentioned reasons and previous research achievements into account, a numerical simulation of the dimension, slots spacing, suction and injection area location, and other parameters was performed. The purpose of this investigation is to study the effect of surface suction and injection on controlling the flow over a specific airfoil. The case studied is the flow field over a subsonic airfoil with suction and injection slots. The investigation is accomplished experimentally. In order to study the effect of suction and injection, four slots are created in the airfoil suction side. Through these slots a secondary flow is injected to the main flow. In other test case a small amount of air is omitted from main flow by suction.



## **1.2 Objectives of the Research Work:**

The objectives of this project work are as follows:

- i) To develop a sub-sonic flow separation control mechanism that could increase the lift force with decrease of the drag force of circular-arc airfoil and thereby reduces total energy consumption.
- ii) To design and construct a mechanism that could generate suction and injection to control the flow over a specific airfoil along slots and holes.
- iii) To investigate the aerodynamic characteristics of an airfoil attached with the flow separation control mechanism

## **1.3 Background**

Fluid flow separation can be controlled by various ways such as motion of the solid wall, slit suction, tangential blowing and suction, continuous suction and blowing by external disturbances etc. These are ancient methods. The modern techniques are the use of surface injection in a multistage compressor, continuous injection and suction of fluid, steady and pulsed jets, oscillatory fluid injection, dielectric barrier discharge plasma actuators, synthetic jet etc.

### **1.3.1 Motion of the solid wall**

One optimal method of avoiding separation would be to completely prevent the formation of a boundary layer. Since the boundary layer owes its existence to the velocity difference between the wall and the outer flow (no-slip condition) it could be eliminated altogether by ensuring that the velocity difference is removed. This can be achieved by moving the wall along with the flow. A moving wall can be most simply realized in the rotation of a circular cylinder in a flow. On the upper side where the direction of flow and the direction of rotation are the same, the separation of the boundary layer is completely avoided. The flow field is unsymmetrical. The inviscid outer flow corresponds to the cylindrical flow with circulation. This flow produces a transverse force known as Magnus effect.

### **1.3.2 Slit Suction**

Slit suction artificially influenced the boundary layer. The flow follows along the surface of the body where the suction is applied for a considerable distance thus preventing separation. The consequence of this is that the drag is greatly decreased. Simultaneously, because the flow is not symmetric, a transverse force is produced. The application of slit suction to a strongly expanding diffuser has been demonstrated, when suction was applied through two slits on each of the two sides, the separation of the flow was completely prevented. The effect of slit suction is essentially based on a change in the velocity distribution of the outer flow. The usual distribution of the inviscid flow is superimposed on the velocity distribution of the sink flow coming from the practically point shaped at the suction slit. This accelerates the flow in front of the suction slit and thus prevents separation. Behind the slit, the sink indeed decelerates the outer flow. Slit suction often used in the past in the development of airfoils to reduce the drag and to increase the drag.

### **1.3.3 Tangential blowing and suction**

A further way of preventing separation consists of supplying additional energy to the particles in the fluid which are low in energy in the boundary layer. This can be achieved by tangentially blowing higher velocity fluid out from inside the body. The danger of separation is removed by the supply of kinetic energy to the boundary layer. The effectiveness of wing flaps can be greatly improved if fluid is tangentially blown out just in front of the flap. If the intensity of the blown jet is high enough, even the lift predicted by potential theory can be surpassed. The so-called jet flap effect then causes super circulation. The separation of the boundary layer can also be prevented by tangential suction. The low energy fluid in the boundary layer is removed by suction before it can separate. Behind the suction slit, a new boundary layer forms which can overcome a certain pressure increase. If the slit is arranged suitably, in certain circumstances the flow will not separate at all.

### **1.3.4 Continuous suction and blowing**

If the wall is permeable and can therefore let the fluid through, the boundary layer can be controlled by continuous suction or blowing. Separation can be prevented by suction



since the low energy fluid in the boundary layer is removed. In contrast, the wall shear stress and therefore the friction drag can be reduced by blowing. The most important application of blowing is in so called transpiration cooling. If a different fluid is injected, a binary boundary layer occurs. As well as velocity and temperature fields, this boundary layer also has a concentration field. The stability of the boundary layer and the transition to turbulence are also considerably influenced by continuous suction and blowing. Suction always stabilizes the boundary layer.

### **1.3.5 Using Vortex Generator Jets**

Flow separation is mostly an undesirable phenomenon and boundary layer control is an important technique for flow separation problems on airfoils and in diffusers. The vortex generator jet method is one of the boundary layer control technique and an active control technique which provides a time-varying control action to optimize performance under a wide range of flow conditions because the strength of longitudinal vortices can be adjusted by varying the jet speed. In this study, an adaptive separation control system using vortex generator jets with rectangular orifices has been developed. The separation control system can be practically applied to the flow separation control of a two-dimensional diffuser. It was confirmed that our separation control system could adaptively suppress flow separation for the flow fields caused by some changes in free stream velocity and the divergence angle of the diffuser. Furthermore, we developed the system which starts the jet blowing just before the onset of separation.

### **1.3.6 Pulse Jet**

Direct numerical simulation (DNS) for flow separation and transition around a NACA-0012 airfoil with an attack of angle ( $\alpha$ ) of  $4^\circ$  and Reynolds number of 100,000 has been reported before. The details of flow separation, formation of the detached shear layer, Kelvin-Helmholtz instability (inviscid shear layer instability) and vortex shedding, interaction of nonlinear waves, breakdown, and re-attachment are obtained and analyzed. The power spectral density of pressure shows the low frequency of vortex shedding caused by the Kelvin-Helmholtz instability still dominates from the leading edge to trailing edge. Based on understanding on the flow separation mechanism, it is tried to reveal the mechanism of the flow separation control using blowing jets and then optimize the jets. The effects of different unsteady blowing jets on the surface at the

location just before the separation points are studied. The length of separation bubble is significantly reduced (almost removed) after unsteady blowing technology is applied.

### **1.3.7 Acoustically Active Surfaces**

In order to develop a mechanically simple and robust actuator for active flow separation control on axial compressor blades, three different types of acoustic transducers were tested in a wind tunnel. Flow separation on a cylinder in cross flow was used. The first transducer had an internally mounted acoustic speaker blowing through a slot. It could control flow separation only for low Reynolds number laminar flows. A flush mounted high-frequency circular piezo-electric transducer was tried next. It was marginally effective only around the laminar-turbulent transition regime. Since it could not focus the perturbations over a small area, the acoustosurf was developed next. It consisted of an array of flush mounted narrow strip shaped acoustic transducers capable of detecting surface pressure fluctuations prior to separation. When the appropriate strips were excited at the predominant fluctuation frequency, separation was delayed for transitional and tripped flows. It is believed that the acoustosurf produces a synergistic interaction between roughness, surface compliance and acoustic radiation to redirect the kinetic energy of the flow by exploiting flow instabilities. Negligible power is therefore needed to operate the acoustosurf. This has attracted the attention of several aircraft manufacturers.

### **1.3.8 Synthetic jet**

Circular cylinder separation control and flow structure influenced by the synthetic jet have been experimentally investigated in a water channel. The synthetic jet issues from a slot and ejects toward upstream from the front stagnation point of the cylinder. It has been found that, similar to the traditional synthetic jet which is positioned near the separation point or inside the separation region, the present synthetic jet arrangement constitutes an efficient way to control flow separation of the circular cylinder.

## CHAPTER II

### LITERATURE REVIEW

#### 2.1 Historical Background

Flow control involves passive or active devices to effect a beneficial change in wall-bounded or free-shear flows. Whether the task is to delay/advance transition, to suppress/enhance turbulence or to prevent/provoke separation, useful end results include drag reduction, lift enhancement, mixing augmentation and flow-induced noise suppression. Broadly, there are perhaps five distinct eras in the development of the art and science of this challenging albeit very useful field of research and technology: The empirical era (prior to 1900); the scientific era (1900-1940); the World War II era (1940-1970); the energy crisis era (1970-1990); and the 1990s and beyond. The art of flow control probably has its roots in prehistoric times when streamlined spears, sickle-shaped boomerangs, and fin-stabilized arrows evolved empirically by archaic Homo sapiens. Relatively soon after the dawn of civilization and the establishment of an agriculture way of life 8,000 years ago, complex systems of irrigation were built along inhabited river valleys to control the water flow, thus freeing man from the vagaries of the weather. For centuries, farmers knew the value of windbreaks to keep top soil in place and to protect fragile crops. The science of flow control originated with Prandtl [1], who, in a mere 8-page manuscript, introduced the boundary layer theory, explained the physics of the separation phenomena and described several experiments in which a boundary layer was controlled. Thus the birth of the scientific method is to control a flow field. Slowly but surely, the choice of flow control devices is no longer a trial and error feat, but physical reasoning and even first principles are more often than not used for rational design of such artifacts. Stimulated by the Second World War and the subsequent cold war, that trend accelerated significantly during the third era (1940-1970). Military needs of the superpowers dictated the development of fast, highly maneuverable, efficient aircraft, missiles, ships, submarines and torpedoes, and flow control played a major role in achieving these goals. Laminar flow control and polymer drag-reduction are notable achievements during this era. Partial summaries of flow control research during this period are contained within the books edited by Lachmann (1961) and Wells (1969). The energy crises exemplified by the 1973 Arab oil embargo brought about a noticeable shift of interest from the military sector to the civilian one.

During the period 1970-1990, government agencies and private corporations around the world but particularly in the industrialized countries invested valuable resources searching for methods to conserve energy, and hence drag reduction for civilian air, sea and land vehicles, for pipelines and for other industrial devices was emphasized. The availability of fast, inexpensive computers made it possible to simulate numerically complex flow situations that have not been approachable analytically. Some control strategies, for example transition-delaying compliant coatings [3], were rationally optimized using computational fluid dynamics. Large-eddy breakup devices (LEBUs) and riblets are examples of control methods developed during this period to reduce skin-friction drag in turbulent boundary layers. Good sources of information on these and other devices introduced during the fourth era are the books edited by Hough , Bushnell and Hefner [6], and Barnwell and Hussaini [5]. Numerous meetings devoted to flow control, particularly drag reduction, were held during this period. Plentiful fuel supplies during the 1990s and the typical short memory of the long gas lines during 1973 have, unfortunately, somewhat dulled the urgency and enthusiasm for energy conservation research as well as practice. For the 1990s and beyond, more complex reactive control devices, geared specifically towards manipulating the omnipresent coherent structures in transitional and turbulent shear flows [7], are pursued by several researchers. Theoretical advances in chaos control and developments of micro electromechanical systems (MEMS) and neural networks should help such efforts. Papers specifically addressing reactive control strategies include those by Moin and Bewley [8], and Gad-el-Hak [9].

## 2.2 Flow Phenomena

In physics and fluid mechanics, a boundary layer is that layer of fluid in the immediate vicinity of a bounding surface. In the Earth's atmosphere, the planetary boundary layer is the air layer near the ground affected by diurnal heat, moisture or momentum transfer to or from the surface. On an aircraft wing the boundary layer is the part of the flow close to the wing. The boundary layer effect occurs at the field region in which all changes occur in the flow pattern. The boundary layer distorts surrounding non-viscous flow. It is a phenomenon of viscous forces. This effect is related to the Reynolds number. Laminar boundary layers come in various forms and can be loosely classified



according to their structure and the circumstances under which they are created. The thin shear layer which develops on an oscillating body is an example of a Stokes boundary layer, whilst the Blasius boundary layer refers to the well-known similarity solution for the steady boundary layer attached to a flat plate held in an oncoming unidirectional flow. When a fluid rotates, viscous forces may be balanced by the Coriolis effect, rather than convective inertia, leading to the formation of an Ekman layer. Thermal boundary layers also exist in heat transfer. Multiple types of boundary layers can coexist near a surface simultaneously.

The aerodynamic boundary layer was first defined by Ludwig Prandtl in a paper presented [1] at the third International Congress of Mathematicians in Heidelberg, Germany. It allows aerodynamicists to simplify the equations of fluid flow by dividing the flow field into two areas: one inside the boundary layer, where viscosity is dominant and the majority of the drag experienced by a body immersed in a fluid is created and one outside the boundary layer where viscosity can be neglected without significant effects on the solution. This allows a closed-form solution for the flow in both areas, which is a significant simplification over the solution of the full Navier-Stokes equations. The majority of the heat transfer to and from a body also takes place within the boundary layer, again allowing the equations to be simplified in the flow field outside the boundary layer.

The thickness of the velocity boundary layer is normally defined as the distance from the solid body at which the flow velocity is 99% of the free stream velocity, that is, the velocity that is calculated at the surface of the body in an inviscid flow solution. An alternative definition, the displacement thickness, recognizes the fact that the boundary layer represents a deficit in mass flow compared to an inviscid case with slip at the wall. It is the distance by which the wall would have to be displaced in the inviscid case to give the same total mass flow as the viscous case. The no-slip condition requires the flow velocity at the surface of a solid object be zero and the fluid temperature be equal to the temperature of the surface. The flow velocity will then increase rapidly within the boundary layer. The thermal boundary layer thickness is similarly the distance from the body at which the temperature is 99% of the temperature found from an inviscid solution. The ratio of the two thicknesses is governed by the Prandtl number. If the Prandtl number is 1, the two boundary layers are the same thickness. If the Prandtl

number is greater than 1, the thermal boundary layer is thinner than the velocity boundary layer. If the Prandtl number is less than 1, which is the case for air at standard conditions, the thermal boundary layer is thicker than the velocity boundary layer.

In high-performance designs, such as sailplanes and commercial transport aircraft, much attention is paid to controlling the behavior of the boundary layer to minimize drag. Two effects have to be considered. First, the boundary layer adds to the effective thickness of the body, through the displacement thickness, hence increasing the pressure drag. Secondly, the shear forces at the surface of the wing create skin friction drag.

At high Reynolds numbers, typical of full-sized aircraft, it is desirable to have a laminar boundary layer. This results in a lower skin friction due to the characteristic velocity profile of laminar flow. However, the boundary layer inevitably thickens and becomes less stable as the flow develops along the body, and eventually becomes turbulent, the process known as boundary layer transition. One way of dealing with this problem is to suck the boundary layer away through a porous surface. This can result in a reduction in drag, but is usually impractical due to the mechanical complexity involved and the power required to move the air and dispose of it. Natural laminar flow is the name for techniques pushing the boundary layer transition aft by shaping of an aerofoil or a fuselage so that their thickest point is aft and less thick. This reduces the velocities in the leading part and the same Reynolds number is achieved with a greater length.

At lower Reynolds numbers, such as those seen with model aircraft, it is relatively easy to maintain laminar flow. This gives low skin friction, which is desirable. However, the same velocity profile which gives the laminar boundary layer its low skin friction also causes it to be badly affected by adverse pressure gradients. As the pressure begins to recover over the rear part of the wing chord, a laminar boundary layer will tend to separate from the surface. Such flow separation causes a large increase in the pressure drag, since it greatly increases the effective size of the wing section. In these cases, it can be advantageous to deliberately trip the boundary layer into turbulence at a point prior to the location of laminar separation, using a turbulator. The fuller velocity profile of the turbulent boundary layer allows it to sustain the adverse pressure gradient without separating. Thus, although the skin friction is increased, overall drag is

decreased. This is the principle behind the dimpling on golf balls, as well as vortex generators on aircraft. Special wing sections have also been designed which tailor the pressure recovery so laminar separation is reduced or even eliminated. This represents an optimum compromise between the pressure drag from flow separation and skin friction from induced turbulence.

### **2.2.1 Laminar flow**

Laminar flow, sometimes known as streamline flow, occurs when a fluid flows in parallel layers, with no disruption between the layers. In fluid dynamics, laminar flow is a flow regime characterized by high momentum diffusion and low momentum convection. It is the opposite of turbulent flow. In nonscientific terms laminar flow is "smooth," while turbulent flow is "rough".

The dimensionless Reynolds number is an important parameter in the equations that describe whether flow conditions lead to laminar or turbulent flow. In the case of flow through a straight pipe with a circular cross-section, Reynolds numbers of less than 2300 are generally considered to be of a laminar type, however, the Reynolds number upon which laminar flows become turbulent is dependent upon the flow geometry. When the Reynolds number is much less than 1, Creeping motion or Stokes flow occurs. This is an extreme case of laminar flow where viscous (friction) effects are much greater than inertial forces. For example, consider the flow of air over an airplane wing. The boundary layer is a very thin sheet of air lying over the surface of the wing (and all other surfaces of the airplane). Because air has viscosity, this layer of air tends to adhere to the wing. As the wing moves forward through the air, the boundary layer at first flows smoothly over the streamlined shape of the airfoil. Here the flow is called laminar and the boundary layer is a laminar layer.

### **2.2.2 Transient flow**

Transient flow is such a flow where the velocity and pressure changes over time. Transient flows usually occur during the starting or stopping of a pump, the opening or closing of a tank, or simple changes in tank levels. Transient flow usually refers to surge or water hammer. The main reason transient flow can be a problem is it can cause pressure that would exceed the limits of pipes, fittings, etc. The dimensionless

Reynolds number is an important parameter in the equations that describe whether flow conditions lead to laminar, transient or turbulent flow. The region in between ( $2100 < Re < 4000$ ) is called the transition region.

### **2.2.3 Turbulent flow**

In fluid dynamics, turbulence or turbulent flow is a fluid regime characterized by chaotic, stochastic property changes. This includes low momentum diffusion, high momentum convection, and rapid variation of pressure and velocity in space and time. Flow that is not turbulent is called laminar flow. While there is no theorem relating Reynolds number to turbulence, flows with high Reynolds numbers usually become turbulent, while those with low Reynolds numbers usually remain laminar. For pipe flow, a Reynolds number above about 4000 will most likely correspond to turbulent flow, while a Reynold's number below 2100 indicates laminar flow. The region in between ( $2100 < Re < 4000$ ) is called the transition region. In turbulent flow, unsteady vortices appear on many scales and interact with each other. Drag due to boundary layer skin friction increases. The structure and location of boundary layer separation often changes, sometimes resulting in a reduction of overall drag. Although laminar-turbulent transition is not governed by Reynolds number, the same transition occurs if the size of the object is gradually increased, or the viscosity of the fluid is decreased, or if the density of the fluid is increased.

Turbulence causes the formation of eddies of many different length scales. Most of the kinetic energy of the turbulent motion is contained in the large scale structures. The energy "cascades" from these large scale structures to smaller scale structures by an inertial and essentially inviscid mechanism. This process continues, creating smaller and smaller structures which produces a hierarchy of eddies. Eventually this process creates structures that are small enough that molecular diffusion becomes important and viscous dissipation of energy finally takes place. The scale at which this happens is the Kolmogorov length scale.

Turbulent diffusion is usually described by a turbulent diffusion coefficient. This turbulent diffusion coefficient is defined in a phenomenological sense, by analogy with the molecular diffusivities, but it does not have a true physical meaning, being dependent on the flow conditions, and not a property of the fluid, itself. In addition, the



turbulent diffusivity concept assumes a constitutive relation between a turbulent flux and the gradient of a mean variable similar to the relation between fluxes and gradient that exists for molecular transport. In the best case, this assumption is only an approximation. Nevertheless, the turbulent diffusivity is the simplest approach for quantitative analysis of turbulent flows, and many models have been postulated to calculate it. For instance, in large bodies of water like oceans this coefficient can be found using Richardson's four-third power law and is governed by the random walk principle. In rivers and large ocean currents, the diffusion coefficient is given by variations of Elder's formula. When designing piping systems, turbulent flow requires a higher input of energy from a pump (or fan) than laminar flow. However, for applications such as heat exchangers and reaction vessels, turbulent flow is essential for good heat transfer and mixing.

#### **2.2.4 Compressible Flow**

Compressible flow theory is distinguished from incompressible flow theory in that the density can no longer be considered a constant. As such, where incompressible flow theory is governed mainly by the conservation of mass and conservation of momentum equations, compressible flows require that the conservation of energy and conservation of entropy equations be solved simultaneously. Maintaining assumption of a calorically perfect gas, these equations can be solved to obtain temperature, pressure and density profiles that vary with local Mach number.

When the Mach number of the flow is high enough so that the effects of compressibility can no longer be neglected as the flow will even out density differences. Below Mach 0.3 fluid flows experience less than a 5% change in density.

#### **2.2.5 Incompressible Flow**

In fluid mechanics or more generally continuum mechanics, an incompressible flow is solid or fluid flow in which the divergence of velocity is zero. This is more precisely termed isochoric flow. It is an idealization used to simplify analysis. In reality, all materials are compressible to some extent. Note that isochoric refers to flow, not the material property. This means that under certain circumstances, a compressible material

can undergo (nearly) incompressible flow. However, by making the 'incompressible' assumption, one can greatly simplify the equations governing the flow of the material.

### **2.2.6 Couette Flow**

In fluid dynamics, Couette flow refers to the laminar flow of a viscous fluid in the space between two parallel plates, one of which is moving relative to the other. The flow is driven by virtue of viscous drag force acting on the fluid and the applied pressure gradient parallel to the plates. This type of flow is named in honor of Maurice Marie Alfred Couette, a Professor of Physics at the French university of Angers in the late 19th century.

### **2.2.7 Secondary Flow**

In fluid dynamics, a secondary flow is a relatively minor flow superimposed on the primary flow, where the primary flow usually matches very closely the flow pattern predicted using simple analytical techniques and assuming the fluid is inviscid. (An inviscid fluid is a theoretical fluid having zero viscosity.)

The primary flow of a fluid, particularly in the majority of the flow field remote from solid surfaces immersed in the fluid, is usually very similar to what would be predicted using the basic principles of physics, and assuming the fluid is inviscid. However, in real flow situations, there are regions in the flow field where the flow is significantly different in both speed and direction to what is predicted for an inviscid fluid using simple analytical techniques. The flow in these regions is the secondary flow. These regions are usually in the vicinity of the boundary of the fluid adjacent to solid surfaces where viscous forces are at work, such as in the boundary layer.

## **2.3 Unifying Principles**

An external wall-bounded flow, such as that developing on the exterior surface of an aircraft or a submarine, can be manipulated to achieve transition delay, separation postponement, lift increase, skin-friction and pressure drag reduction, turbulence augmentation, heat transfer enhancement, or noise suppression. These objectives are not necessarily mutually exclusive. For example, by maintaining as much of a boundary layer in the laminar state as possible, the skin-friction drag and the flow-induced noise

are reduced. However, a turbulent boundary layer is in general more resistant to separation than a laminar one. By preventing separation, lift is enhanced and form drag is reduced. Moreover, mixing and heat transfer are enhanced by the turbulence. The challenge in choosing a flow control scheme is of course to achieve a beneficial goal at a minimum cost, without adversely affecting another goal. An ideal method of control that is simple is inexpensive to build and to operate, and does not have any trade-off does not exist and the skilled engineer have to make continuous compromises to achieve a particular design objective.

There are different classification schemes for flow control methods. One is to consider whether the technique is applied at the wall or away from it. Surface parameters that can influence the flow include roughness, shape, curvature, rigid-wall motion, compliance, temperature, and porosity. Heating and cooling of the surface can influence the flow via the resulting viscosity and density gradients. Mass transfer can take place through a porous wall or a wall with slots. Suction and injection of primary fluid can have significant effects on the flow field, influencing particularly the shape of the velocity profile near the wall and thus the boundary layer susceptibility to transition and separation. Different additives, such as polymers, surfactants, micro-bubbles, droplets, particles, dust or fibers, can also be injected through the surface in water or air wall bounded flows. Control devices located away from the surface can also be beneficial. Large-eddy breakup devices (also called outer-layer devices, or OLDs), acoustic waves bombarding a shear layer from outside, additives introduced in the middle of a shear layer, manipulation of free stream turbulence levels and spectra, gust, and magneto- and electro-hydrodynamic body forces are examples of flow control strategies applied away from the wall.

A second scheme for classifying flow control methods considers energy expenditure and the control loop involved. As shown in the Fig 2.1, a flow control device can be passive, requiring no auxiliary power, or active, requiring energy expenditure. As for the action of passive devices, some prefer to use the term flow management rather than flow control [10], reserving the latter terminology for dynamic processes. Active control is further divided into predetermined or reactive. Predetermined control includes the application of steady or unsteady energy input without regard to the particular state of the flow. The control loop in this case is open as shown in Fig 2.2(a), and no sensors are required.

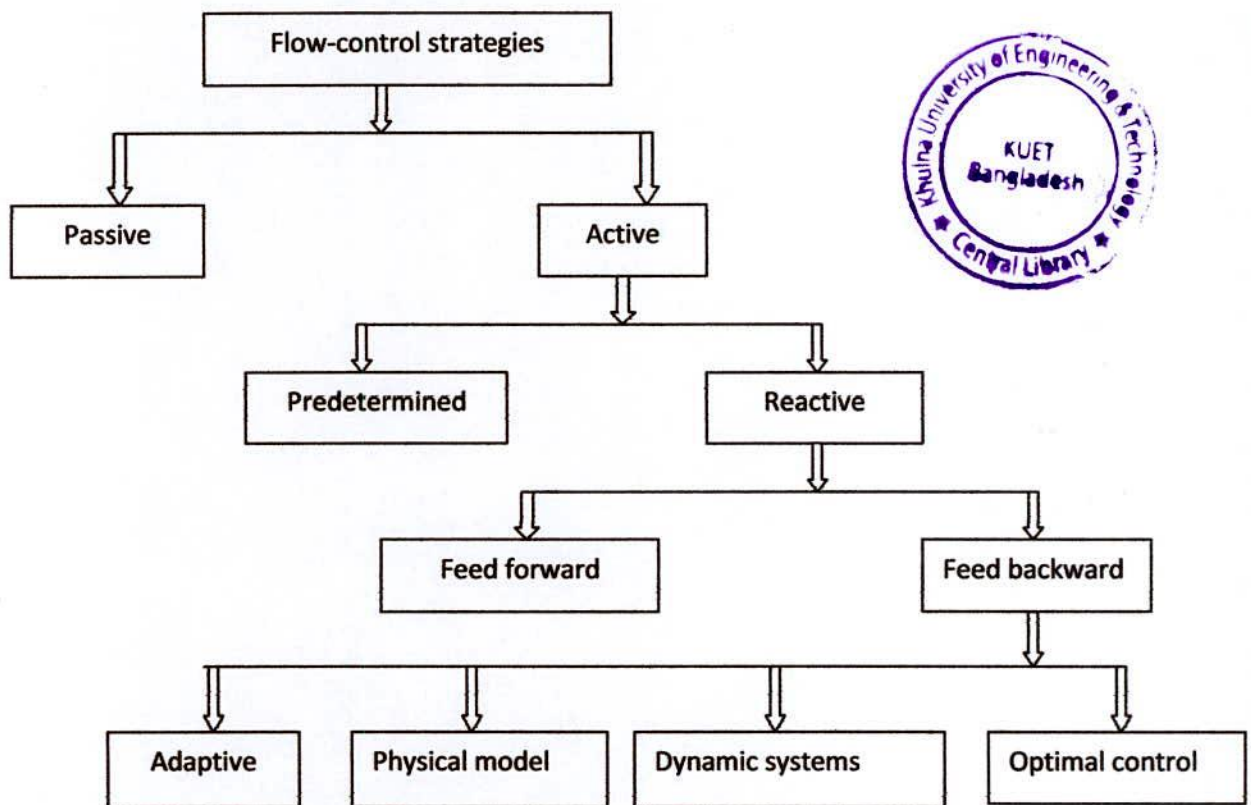


Figure 2.1 Classifications of Flow Control Strategies

Reactive control is a special class of active control where the control input is continuously adjusted based on measurements of some kind. The control loop in this case can either be an open, feedforward one (Fig 2.2 b) or a closed, feedback loop (Fig 2.2 c). Classical control theory deals, for the most part, with reactive control.

The distinction between feedforward and feedback is particularly important when dealing with the control of flow structures which convect over stationary sensors and actuators. In feedforward control, the measured variable and the controlled variable differ. For example, the pressure or velocity can be sensed at an upstream location, and the resulting signal is used together with an appropriate control law to trigger an actuator which in turn influences the velocity at a downstream position. Feedback control, on the other hand, necessitates that the controlled variable be measured, fed back and compared with a reference input. Reactive feedback control is further

classified into four categories: Adaptive, physical model-based, dynamical systems-based and optimal control [8].

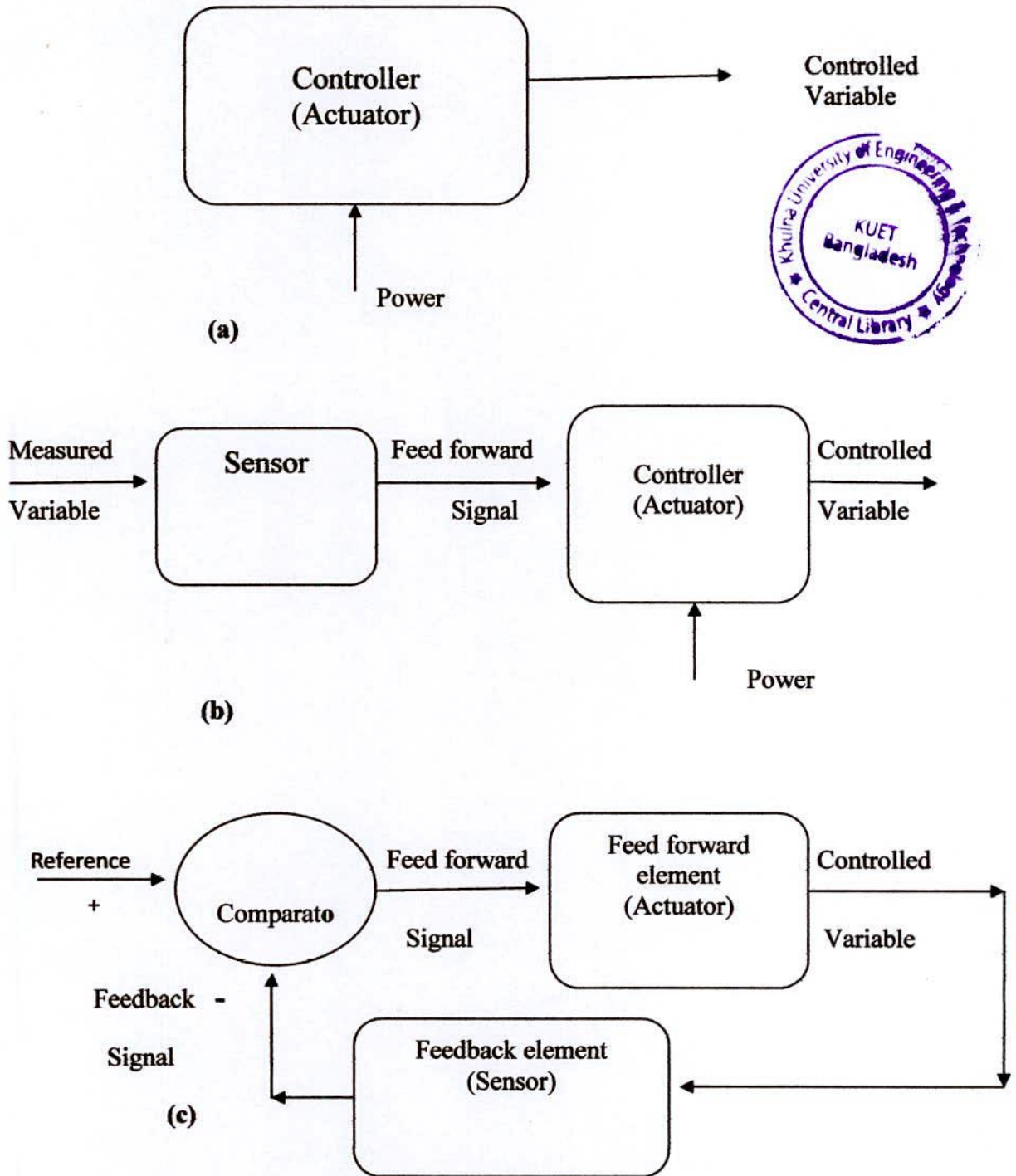


Figure 2.2 Different Control Loops for Active Flow Control.

Flow control devices can alternatively target certain scales of motion rather than globally changing the velocity profile. Polymers and riblets, for example, appear to selectively damp only the small dissipative eddies in turbulent wall-bounded flows. These eddies are responsible for the (instantaneous) inflectional profile and the secondary instability in the buffer zone, and their suppression leads to increased scales, a delay in the reduction of the velocity-profile slope, and consequent thickening of the wall region. In the buffer zone, the scales of the dissipative and energy containing eddies are roughly the same and, hence, the energy containing eddies will also be suppressed resulting in reduced Reynolds stress production, momentum transport and skin friction.

### **2.3.1 Active Control**

In contrast, active control devices use energy such as surface suction or injection. Active separation control is considered one of the enabling technologies for the next generation of hybrid wing body vehicles. For this reason, the National Aeronautics and Space Administration's Subsonic Fixed Wing Project funds both internal and external research in this area. This research is fundamental, long-term research focused on obtaining a better understanding of the physics governing active separation control. Natural laminar flow implies delaying transition via controlling the body shape to provide long runs of favorable pressure-gradient. This has been applied since the 1930s on airfoil sections to achieve lower skin friction drag. The principal types of active laminar-flow control are surface cooling and removal of a small amount of air from the boundary layer by suction. Generally, in surface injection, a secondary flow is injected from miniature openings or slots on the surface. In surface suction, the air is sucked from them. For highly swept wings, only suction can control sweep-induced cross-flow disturbances that promote boundary layer transition from laminar to turbulent.

### **2.3.2 Passive Control**

Passive control devices are those, which are not energy consumptive. They mainly affect the flow by the geometry of the airfoil. For example the presence of friction in the flow causes a shear stress at the surface of the body, which in turn contributes to the

aerodynamic drag of the body i.e. skin frictions drag. However, friction also causes another phenomenon called flow separation, which in turn creates another source of aerodynamic drag called pressure drag due to separation. From a fluid dynamist's point of view, the performance of an aircraft is essentially controlled by the development of the boundary layer on its surface and its interaction with the mean flow. This interaction decides the pressure distribution on the airfoil surface, and subsequently the aerodynamic loads on the wing.

### **2.3.3 Reactive Control**

Numerous methods of flow control have already been successfully implemented in practical engineering devices. Yet, limitations exist for some familiar control techniques when applied to specific situations. For example, in attempting to reduce the drag or enhance the lift of a body having a turbulent boundary layer using global suction, the penalty associated with the control device often exceeds the saving derived from its use. What is needed is a way to reduce this penalty to achieve a more efficient control. Reactive control geared specifically towards manipulating the coherent structures in transitional and turbulent shear flows, though considerably more complicated than passive control or even predetermined active control, has the potential to do just that. As will be argued in this and the following three sections, future systems for control of transitional and turbulent flow in general and turbulent boundary layers in particular could greatly benefit from the merging of the science of chaos control and the technologies of micro fabrication and neural networks. Such systems are envisaged as consisting of a large number of intelligent, communicative wall sensors and actuators arranged in a checkerboard pattern and targeted towards controlling certain quasi-periodic, dynamically significant coherent structures present in the wall region.

The recent numerical experiments also validate the concept of targeting suction/injection to specific near-wall events in a turbulent channel flow [11]. Based on complete interior flow information, their direct numerical simulations indicate a 20% net drag reduction accompanied by significant suppression of the near-wall structures and the Reynolds stress throughout the entire wall-bounded flow. When only wall information was used, a drag reduction of 6% was observed; a rather disappointing result considering that sensing and actuation took place at every grid point along the

computational wall. In a practical implementation of this technique, even fewer wall sensors would perhaps be available, measuring only a small subset of the accessible information and thus requiring even more sophisticated control algorithms to achieve the same degree of success. Time sequences of the numerical flow field indicate the presence of two distinct drag-reducing mechanisms when selective suction/injection is used. First, deterring the sweep motion, without modifying the primary streamwise vortices above the wall, and consequently moving the high-shear regions from the surface to the interior of the channel, thus directly reducing the skin friction. Secondly, changing the evolution of the wall vorticity layer by stabilizing and preventing lifting of the near-wall span wise vorticity, thus suppressing a potential source of new stream wise vortices above the surface and interrupting a very important regeneration mechanism of turbulence.

#### **2.3.4 Reactive Feedback Control**

Moin and Bewley categorize reactive feedback control strategies by examining the extent to which they are based on the governing flow equations [8]. Four categories are discerned: adaptive, physical model-based, dynamical systems-based, and optimal control. Note that except for adaptive control, the other three categories of reactive feedback control can also be used in the feed forward mode or the combined feedforward-feedback mode. Also, in a convective environment such as that for a boundary layer, a controller would perhaps combine feed forward and feedback information and may include elements from each of the four classifications. Each of the four categories is briefly described below. Adaptive schemes attempt to develop models and controllers via some learning algorithm without regard to the details of the flow physics. System identification is performed independently of the flow dynamics or the Navier-Stokes equations which govern this dynamics. An adaptive controller tries to optimize a specified performance index by providing a control signal to an actuator. In order to update its parameters, the controller thus requires feedback information relating to the effects of its control. The most recent innovation in adaptive flow control schemes involves the use of neural networks which relate the sensor outputs to the actuator inputs through functions with variable coefficients and nonlinear, sigmoid saturation functions. The coefficients are updated using the so-called back-propagation



algorithm, and complex control laws can be represented with a sufficient number of terms. Hand tuning is required, however, to achieve good convergence properties. The nonlinear adaptive technique has been successfully used by Fan [12], Jacobson and Reynolds [13] to control, respectively, the transition process and the bursting events in turbulent boundary layers. Heuristic physical arguments can instead be used to establish effective control laws. That approach obviously will work only in situations in which the dominant physics are well understood. An example of this strategy is the active cancellation scheme, used by Gad-el-Hak and Blackwelder[14] in a physical experiment and by Choi [11] in a numerical experiment, to reduce the drag by mitigating the effect of near-wall vortices. As mentioned earlier, the idea is to oppose the near-wall motion of the fluid, caused by the stream wise vortices, with an opposing wall control, thus lifting the high-shear region away from the surface and interrupting the turbulence regeneration mechanism.

Finally, optimal control theory applied directly to the Navier-Stokes equations can be used to minimize a cost function in the space of the control. This strategy provides perhaps the most rigorous theoretical framework for flow control. In this method, feedback control laws are derived systematically for the most efficient distribution of control effort to achieve a desired goal. Abergel and Temam [15] developed such optimal control theory for suppressing turbulence in a numerically simulated, two-dimensional Navier-Stokes flow, but their method requires impractical full flow-field information. Choi developed a more practical, wall information-only, sub-optimal control strategy which they applied to the one-dimensional stochastic Burgers equation[16]. Later application of the sub-optimal control theory to a numerically simulated turbulent channel flow is reported by Moin and Bewley [8].

#### **2.4 Wall-Bounded and Free-Shear Flows**

A particular control strategy is chosen based on the kind of flow and the control goal to be achieved. Presence or lack of walls, Reynolds number, Mach number, and the character of the flow instabilities are all important considerations for the type of flow to be controlled.

#### **2.4.1 Inviscid and Viscous Instabilities**

Free-shear flows, such as jets, wakes or mixing layers, are characterized by inflectional mean-velocity profiles and are therefore susceptible to inviscid instabilities. Viscosity is only a damping influence in this case, and the prime instability mechanism is vortical induction. Control goals for such flows include transition delay/advancement, mixing enhancement and noise suppression. External and internal wall-bounded flows, such as boundary layers and channel flows, can too have inflectional velocity profiles, but, in the absence of adverse pressure-gradient and similar effects, are characterized by non-inflectional profiles and viscous instabilities are then to be considered. These kind of viscosity-dominated wall-bounded flows are intrinsically stable and therefore are generally more difficult to control. Free-shear flows and separated boundary layers, on the other hand, are intrinsically unstable and lend themselves more readily to manipulation. Free-shear flows originate from some kind of surface upstream be it a nozzle, a moving body or a splitter plate, and flow control devices can therefore be placed on the corresponding walls albeit far from the fully developed regions. Examples of such control include changing of the geometry of a jet exit from circular to elliptic [17], using periodic suction/injection in the lee side of a blunt body to affect its wake (Williams and Amato, 1989), and vibrating the splitter plate of a mixing layer [18]. These and other techniques are extensively reviewed by Fiedler and Fernholz [19], who offer a comprehensive list of appropriate references, and more recently by Gutmark [20] and Viswanath [21].

#### **2.4.2 Regimes of Reynolds and Mach Numbers**

Reynolds number determines whether the flow is laminar or turbulent. For low-to-moderate Reynolds numbers, the flow is laminar. Because of the nature of their instabilities, free shear flows undergo transition at extremely low Reynolds numbers as compared to wall-bounded flows. Many techniques are available to delay laminar-to-turbulence transition for both kinds of flows, but none would do that to indefinitely high Reynolds numbers. Therefore, for Reynolds numbers beyond a reasonable limit, one should not attempt to prevent transition but rather deal with the ensuing turbulence. Of course early transition to turbulence can be advantageous in some circumstances, for example to achieve separation delay, enhanced mixing or augmented heat transfer. The

task of advancing transition is generally simpler than trying to delay it. Three Reynolds number regimes can be identified for the purpose of reducing skin friction in wall-bounded flows. First, if the flow is laminar, typically at Reynolds numbers based on distance from leading edge  $< 10^6$ , then methods of reducing the laminar shear stress are sought. These are usually velocity-profile modifiers, for example adverse-pressure gradient, injection, cooling (in water) and heating (in air), that reduce the fullness of the profile at the increased risk of premature transition and separation. Secondly, in the range of Reynolds numbers from  $1 \times 10^6$  to  $4 \times 10^7$ , active and passive methods to delay transition as far back as possible are sought. These techniques can result in substantial savings and are broadly classified into two categories: stability modifiers and wave cancellation [22]. The skin-friction coefficient in the laminar flat-plate can be as much as an order of magnitude less than that in the turbulent case. Note, however, that all the stability modifiers, such as favorable pressure-gradient, suction or heating (in liquids), result in an increase in the skin friction over the unmodified Blasius layer. The object is, of course, to keep this penalty below the potential saving; *i.e.*, the net drag will be above that of the flat-plate laminar boundary-layer but presumably well below the viscous drag in the flat-plate turbulent flow. Thirdly, for  $Re > 4 \times 10^7$ , transition to turbulence cannot be delayed with any known practical method without incurring a penalty that exceeds the saving. The task is then to reduce the skin-friction coefficient in a turbulent boundary layer. Relaminarization is an option, although achieving a net saving here is problematic at present [23]. Mach number determines whether the flow is incompressible ( $Ma < 0.3$ ) or compressible ( $Ma > 0.3$ ). The latter regime is further divided into subsonic ( $Ma < 1$ ), transonic ( $0.8 < Ma < 1.2$ ), supersonic ( $Ma > 1$ ), and hypersonic ( $Ma > 5$ ). Each of those flow regimes lends itself to different optimum methods of control to achieve a given goal. Take laminar-to-turbulence transition control as an illustration [6]. During transition, the field of initial disturbances is internalized via a process termed receptivity and the disturbances are subsequently amplified by various linear and nonlinear mechanisms. Assuming that bypass mechanisms, such as roughness or high levels of free stream turbulence, are identified and circumvented, delaying transition then is reduced to controlling the variety of possible linear modes: Tollmien-Schlichting modes, Mach modes, cross flow instabilities and Görtler instabilities. Tollmien-Schlichting instabilities dominate the transition process for two-dimensional boundary layers having  $Ma < 4$ , and are

damped by increasing the Mach number, by wall cooling (in gases), and by the presence of favorable pressure-gradient. Contrast this to the Mach modes which dominate for two-dimensional hypersonic flows. Mach instabilities are also damped by increasing the Mach number and by the presence of favorable pressure-gradient, but are destabilized by wall cooling. Cross flow and Görtler instabilities are caused by, respectively, the development of inflectional cross flow velocity profile and the presence of concave streamline curvature. Both of these instabilities are potentially harmful across the speed range, but are largely unaffected by Mach number and wall cooling. The cross flow modes are enhanced by favorable pressure-gradient, while the Görtler instabilities are insensitive. Suction suppresses, to different degrees, all the linear modes discussed in here.

#### **2.4.3 Convective and Absolute Instabilities**

In addition to grouping the different kinds of hydrodynamic instabilities as inviscid or viscous, one could also classify them as convective or absolute based on the linear response of the system to an initial localized impulse [23]. A flow is convectively unstable if, at any fixed location, this response eventually decays in time. In other words, if all growing disturbances convect downstream from their source. Suppression of convective instabilities is particularly effective when applied near the point where the perturbations originate. If any of the growing disturbances has zero group velocity, the flow is absolutely unstable. This means that the local system response to an initial impulse grows in time. In this case, some of the growing disturbances can travel back upstream and continually disrupt the flow even after the initial disturbance is neutralized. Therefore, absolute instabilities are generally more dangerous and more difficult to control; nothing short of complete suppression will work. In some flows, for example two-dimensional blunt-body wakes, certain regions are absolutely unstable while others are convectively unstable.



#### 2.4.4 Classical Control Tools

We end this section by listing several traditional flow control strategies that are either already in application or are market ready. Natural laminar flow (NLF) implies delaying transition via controlling the body shape to provide long runs of favorable pressure-gradient, and has been applied since the 1930s on airfoil sections to achieve lower skin-friction drag. Laminar flow control (LFC), in contrast, uses suction, wall heating/cooling and other active means of control to suppress the proper instability modes. Though well established in the laboratory and successfully field tested, routine application in the field of the variety of available LFC strategies is awaiting the removal of some technological hurdles related mostly to cost, maintenance and reliability issues [24, 25, and 26]. Compliant coatings offer a rather simple method to delay laminar-to-turbulence transition as well as to interact favorably with a turbulent wall-bounded flow. In its simplest form, the technique is passive, relatively easy to apply to an existing vehicle or device, and perhaps not too expensive. The subject, though periodically discredited/redeemed, has been recently reviewed by Gad-el-Hak [4], who argues that compliant coatings could be market ready with modest additional research effort. Available techniques to reduce skin-friction drag in turbulent wall-bounded flows include riblets and polymer. The first two yield only modest drag reduction of the order of 10%, while polymer additives result in substantial reduction of as much as 80%. Polymers, appropriate only for hydrodynamic flows, are occasionally utilized in practical pipelines, for example in the 800-mile Trans-Alaskan Pipeline System (TAPS) that carries crude oil from Prudhoe Bay to the port of Valdez, but the main hurdle for using the strategy for external flows is the cost and weight of the additive to be carried onboard a surface ship or a submarine. Of all the various types of shear-flow control now extant, control of flow separation, historically referred to as boundary-layer control (BLC), is probably the oldest and most economically important [27]. Generally it is desired to postpone separation so that form drag is reduced, stall is delayed, lift is enhanced and pressure recovery is improved. However, in some instances it may be beneficial to provoke separation. For example, to improve the subsonic high-lift performance of an airfoil optimized for high-speed flight, a flap may be used to initiate leading-edge separation followed by reattachment. Flow separation control is currently employed via vortex generators on the wings of most Boeing

aircraft; via blown flaps on older generation supersonic fighters or leading-edge extensions and strakes on newer generations; and via passive bleed in the inlets of supersonic engines on, for example, the SR-71 and Concorde. Emerging control strategies for both steady and unsteady separation include transient suction and microblowing; these are described by, among others, Karim and Acharya [28], Alrefai and Achary [29], and Roos [30]. Future possibilities for aeronautical applications of flow separation control include providing structurally efficient alternatives to flaps or slats; cruise application on conventional takeoff and landing aircraft on thick span loader wings; as well as cruise application on high-speed civil transports for favorable interference wave-drag reduction, increased leading edge thrust, and enhanced fuselage and upper surface lift. In fact, much of the remaining gains to be made in aerodynamics appear to involve various types of flow control, including separated flow control. Typical, in some cases serious, problems associated with flow separation control include parasitic device drag or energy consumption; system weight, volume, complexity, reliability or cost; performance sensitivity to body attitude or orientation; and, especially in the case of the automobile, styling.

## 2.5 Conclusions

The present article reviewed the important advances in the field of flow control that took place during the past few years. An attempt has been made to place the field in a unifying framework and to properly categorize the different control strategies. The complex control schemes, passive as well as active, are more market ready and are also witnessing resurgence of interest.

As is clear from this brief review, there is no lack of flow control methods to achieve a particular goal for free as well as wall-bounded flows across the entire range of Mach and Reynolds numbers. Ranging from simple to complex, from inexpensive to expensive, from passive to active to reactive and from market ready to futuristic, the fluid engineer has a great variety of control devices to choose from. Flow control is most effective when applied near the transition or separation points; in other words, near the critical flow regimes where flow instabilities magnify quickly. Therefore, delaying/advancing laminar-to-turbulence transition and preventing/provoking separation can be readily accomplished. To reduce the skin-friction drag in a non-

separating turbulent boundary layer, where the mean flow is quite stable, is a more challenging problem.

## CHAPTER III

### METHODOLOGY

#### 3.1 Flow separation control mechanism

To control the flow, passive or active devices are used. Passive control devices are those, which are not energy consumptive. They mainly affect the flow by the geometry of the airfoil. In contrast, active control devices use energy such as surface suction or injection. The boundary layer suction is to prevent separation of either of laminar or turbulent layers. The suction removes the retarded air close to the surface, it will remove the cause of separation, and this aspect leads to its use to obtain high lift coefficients from various airfoil configurations. The suction of air from the boundary layer flow into the surface of the body, causes the tired air near the surface being removed and a new boundary layer is started to reform downstream of the suction point with a consequent reduction in drag [31]. Generally, in surface injection, a secondary fluid is injected through miniature openings or slots on the surface. In this separation control, which is due to the complete loss of energy of the air flowing immediately adjacent to the surface, is to energize this tired air by means of blowing a thin, high speed jet into it and improve efficiency that means reduce total consumption of energy by increase lift with decreasing drag force.

In order to study the effect of suction and injection, four inclined internal slots and holes are created in the airfoil suction side. Through these slots and holes a secondary fluid is injected to the main flow of supplying additional energy to the particles in the fluid which are low in energy in the boundary layer. The most important application of injection is in so called transpiration cooling. If a different fluid is injected, a binary boundary layer occurs. As well as velocity and temperature fields, this boundary layer also has a concentration field. In other case a small amount of air is sucked from main flow by suction. The low energy fluid in the boundary layer is removed by suction before it can separate.

In this experiment continuous injection and suction were done by a single cylinder piston mechanism which supplied secondary fluid and sucked low energy fluid from the upper surface of the wing. The experiment was conducted with a model wing constructed with a base profile of a NACA 2415. Each model has a recess cut in the



upper surface, into which a sub-sonic flow separation control mechanism that could generate suction and injection fluid flow over an airfoil. The data of pressure difference was taken by the digital manometer. The pressure co-efficient was measured by following equation-

Co-efficient of Pressure, 
$$C_p = \frac{P - P_\infty}{q_\infty}$$

$$C_p = \frac{P - P_\infty}{\frac{1}{2} \rho_\infty U_\infty^2} \text{----- 3.1}$$



From above equation, the value of  $C_p$  is found and Lift and drag co-efficient are calculated by integrating the pressures over the wing.

Co-efficient of Lift, 
$$C_l = \frac{1}{c} \int_0^c (C_{p_l} - C_{p_u}) dx \text{----- 3.2}$$

Co-efficient of Drag, 
$$C_d = \frac{1}{c} \int_0^c (C_{p_l} - C_{p_u}) dy \text{----- 3.3}$$

All the Co-efficient of  $C_p$ ,  $C_l$ , and  $C_d$  were measured for each of the frequency; the frequency varies with the change of motor speed. The Reduced frequency calculated by the given equation-

Reduced Frequency, 
$$F = \frac{f_e x_R}{U_\infty} \text{----- 3.4}$$

In the case with suction and injection slots, mass flow rate of air is 0.07 kg/Sec from each slot. Nine different angles of attack( $\alpha$ ), 0, 2, 4, 6, 8, 10, 12, 14, and 20 were taken into consideration and three different fluid flow velocities were 4 m/s, 5 m/s, 6 m/s and corresponding Reynolds numbers ( $R_e$ ) were 50000, 62500 and 75000. Four types of frequencies were considered for each angle of attack and velocity.

## CHAPTER IV

### EXPERIMENTAL SETUP AND PROCEDURE

#### 4.1 Introduction

Measurements were carried out in the small subsonic wind tunnel which is located in the Fluid Mechanics Laboratory in the Department of Mechanical Engineering, Khulna University of Engineering & Technology. Two different condition but same dimension models were constructed: for air pressure measurements in the wind. The facilities and the models are here briefly described.

#### 4.2 Wind Tunnel

Wind tunnels can be divided into one of two types: open circuit (also called “straight through”) or closed circuit (also called “return flow”) [32]. Open circuit wind tunnels pull the air from the environment into the tunnel and release the air back into the environment, whereas the closed circuit continually circulates the same air throughout the tunnel. Closed circuit wind tunnels are advantageous over open circuit wind tunnels for the following reasons: the quality of the flow can be easily controlled with screens and corner turning vanes; less energy is required to create an airflow of a given size and velocity; the wind tunnel runs more quietly. The disadvantages are the initial expense of building and need to change the air if it is significantly heated or polluted with smoke from smoke testing or engines [33]. Fortunately, neither of the disadvantages was found. This experiment was carried out by the subsonic open-circuit wind tunnel, it was low-speed wind tunnel installed in 1983 in Fluid Mechanics Lab of Khulna University of Engineering & Technology. To reduce the turbulence level one honeycomb and four nylon-conditioning screens were included in the settling chamber. The test section dimensions were 36 cm x 36 cm x 100 cm and include a movable plexiglass wall for easy access as well as visualization. The tunnel was powered by a 15 hp motor. By changing the power supply of the drive motor the tunnel speed can be varied. It can achieve maximum free-stream velocity of 10 m/s.

The tunnel free stream velocity is obtained by a Pitot tube mounted in middle of the wind tunnel, which is connected to the Digital Electronic Manometer model METRAVI PM-01 NEDA 1604 IEC 6F22 that would provide readout of the static pressure. The

Electronic Manometer has a range of 0-100 bar with an accuracy of 0.05% of the pressure reading and a full-scale resolution of 0.001%.

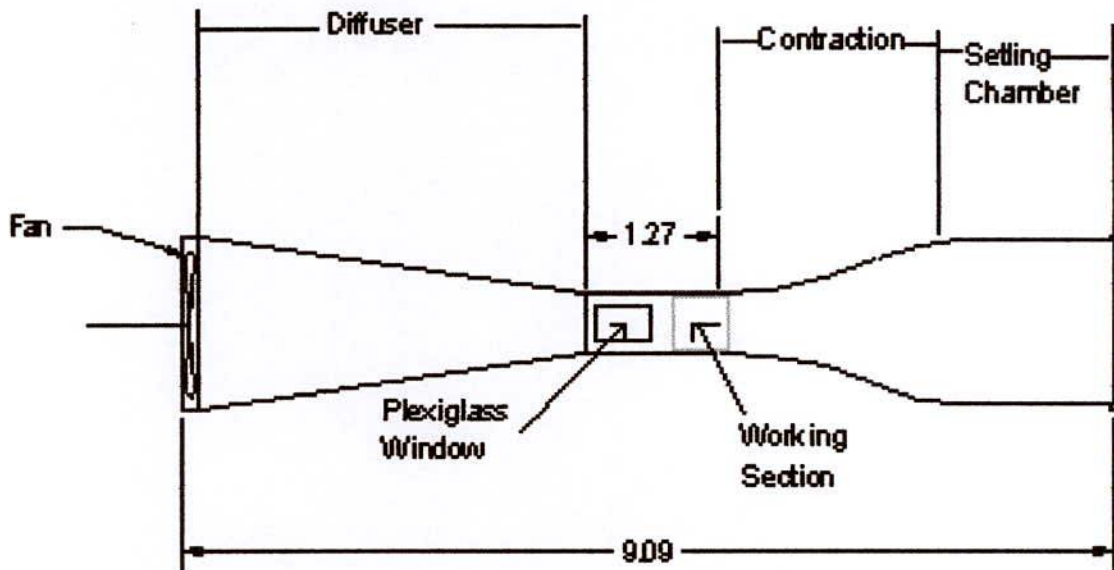


Figure 4.2: Subsonic Wind Tunnel Schematic

#### 4.3 Construction of Model (wing)

Wing is an aerodynamic structure that generates lift when comes in contact with moving air molecules i.e. wind. The lift is generated due to the wing's unique shape. It is curved on the upper surface and is almost flat on the bottom surface. This unusual form causes the air to go faster over the top than the bottom. This difference in speed results in a difference in pressure between the top and the bottom of the wing which exerts an upward net force on the wing. This upward force is called lift.

The amount of lift obtained from the wing depends on the shape of its airfoil and its angle of incidence. There is usually a relationship between the angle at which the wing is permanently inclined to the airplane's longitudinal axis and the amount of lift generated. At small angles, as the angle of attack is increased the lift increases; however at a certain point the drag on the wing dominates the lift and the aircraft goes into stall.

The model used for this phase is a nonsymmetrical NACA 2415 airfoil. The chord length is 200 mm with maximum thickness of 30 mm. Its span is 150 mm. The model was constructed by using light wood. The set-up is built in two separate phases: one is

the buster and motor arrangement, by which flow secondary fluid through the airfoil slot and hole, and other is the body of the airfoil. The first model has no suction and injection slots and the second model, shown in Fig 4.3(a), has four inclined slots by which suction and injection is completed. Third model, shown in Fig 4.3(b) is similar to second model except replacing slots with inclined 1 mm holes. The motor run the buster which sucked fluid from the upper surface and inject secondary fluid by one complete revelation. The buster revolution is change by changing fly wheel diameter of the buster. The secondary fluid injected and sucked by a tube connected buster head and header pipe of the four slots or holes. The chord length of the airfoil is 200mm and the thickness is 30mm.



Figure 4.3(a): Construction of Model NACA 2415 with four slots

The width of each slot is 1mm and diameter of the holes is 1mm and the slots and holes are 30mm apart. Nine different angles of attack, 0, 2, 4, 6, 8, 10, 12, 14, and 20 are taken into consideration and three different fluid flow velocities are 4 m/s, 5 m/s, 6 m/s.

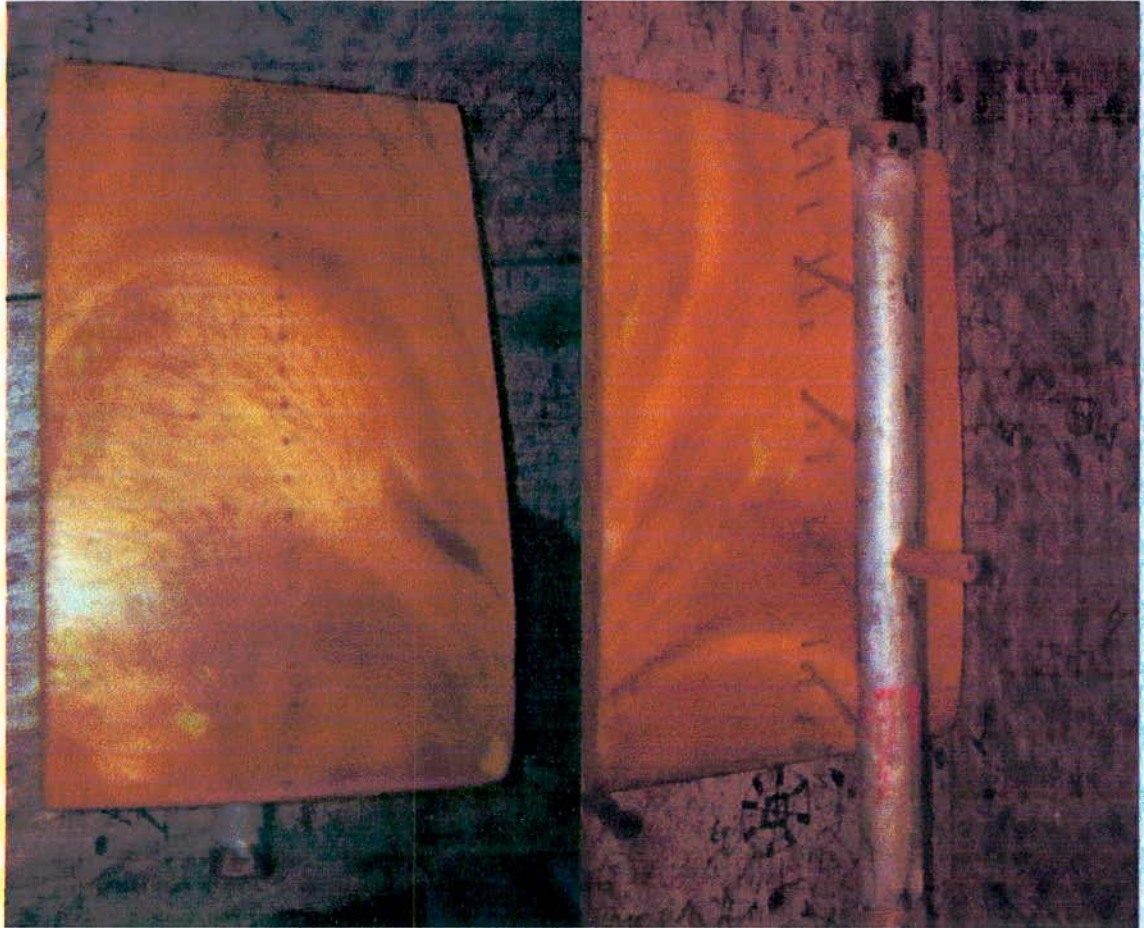


Figure 4.3(b): Construction of Model NACA 2415 with four holes

#### 4.4 Experimental Setup

The experiments were performed in an open-circuit low-speed wind tunnel shown in Fig. 4.4(a), 4.4(b) and 4.4(c) located in the Fluid Mechanics lab of Mechanical Engineering Department of Khulna University of Engineering & Technology. The tunnel had a test section with a  $36\text{ cm} \times 36\text{ cm}$  cross section and all the walls of the test section were optically transparent. Figure 4.4 (d) shows the airfoil NACA 2415 used in the present study.

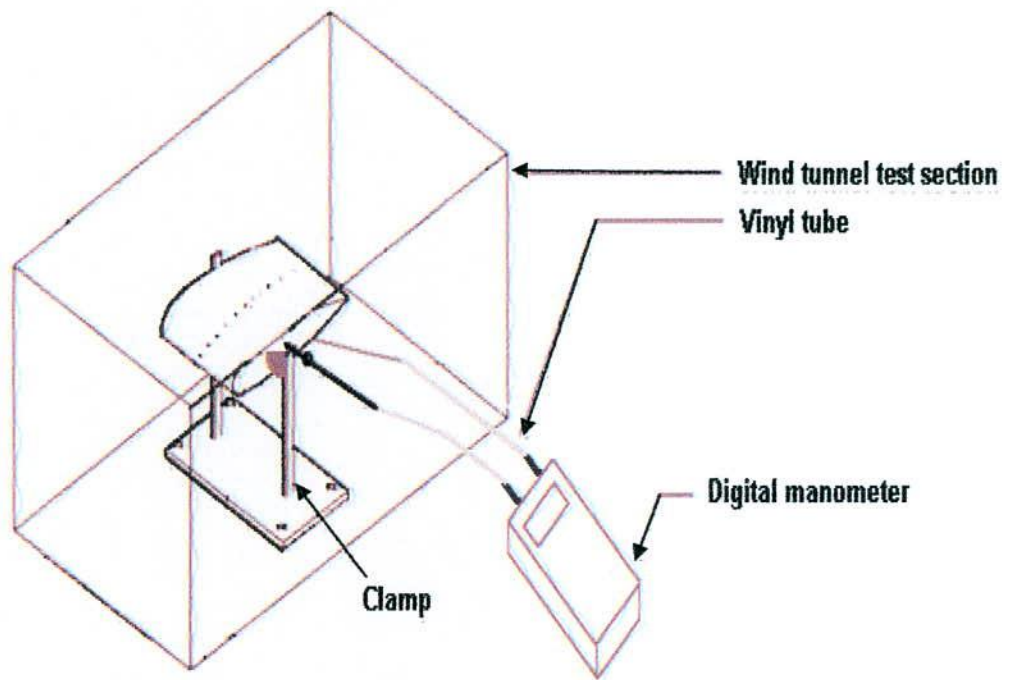


Figure 4.4(a) Experimental set up in schematic drawing



Figure 4.4(b) Experimental set up of model in wing tunnel

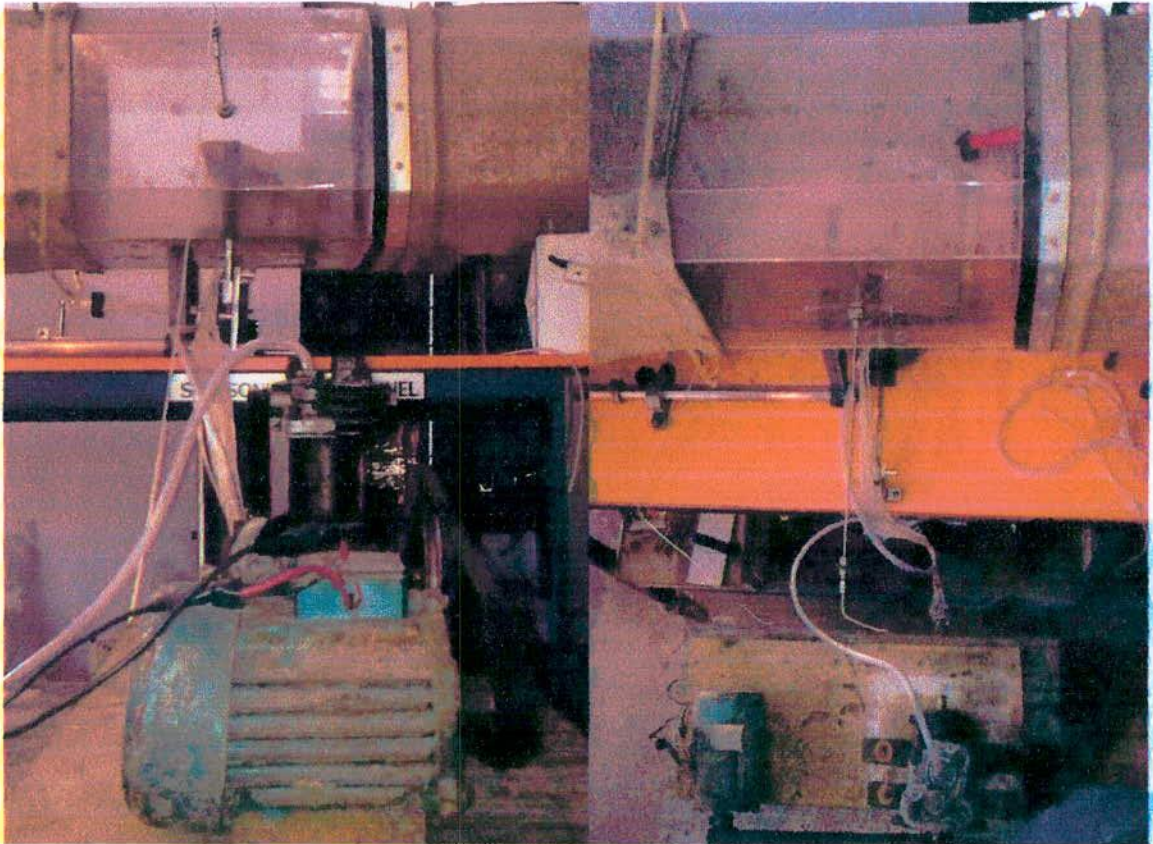


Figure 4.4(c) Experimental set up model with single piston mechanism

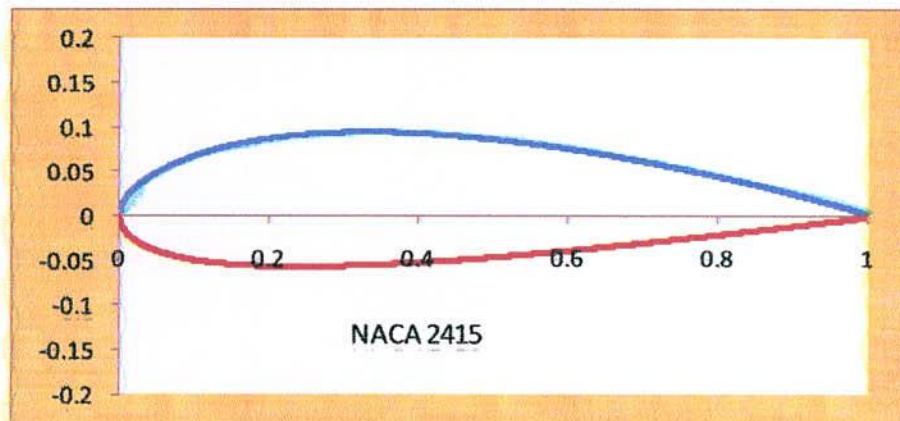


Figure 4.4 (d) Airfoil geometry of NACA 2415

The chord length of the airfoil is 200 mm, i. e.,  $c = 200\text{mm}$  and the maximum thickness of 15% of the chord length. The maximum velocity of the uses wine tunnel is  $U_{\infty} = 10.0$  m/s, which corresponds to a Reynolds number of  $Re = 68,000$  and the set range of angle of attack (AOA) is  $0^{\circ}$  to  $20^{\circ}$  ( zero to twenty degree). Nine different angles of attack, 0, 2, 4, 6, 8, 10, 12, 14, and 20 are taken into consideration and three different

fluid flow velocities are 4 m/s, 5 m/s, 6 m/s. The Experimental study is conducted on three cases in each angle of attack. The three cases are airfoil with surface suction, surface injection and the base airfoil. The term base airfoil is referred to the airfoil without suction or injection.

#### 4.4.1 Pressure Measurement

For the pressure measurement a digital manometer was placed outside of the wind tunnel test section. There were drilled holes vertically in every 10 mm distance of the model and vinyl tubes were placed in these holes. The vinyl tubes were connected between the pressure tubes, set to the model and the digital manometer. The surface pressure of the model varied with respect to chord length scale. The values of surface pressure of the model were measured in accordance with various values of wind tunnel velocity, angle of attack and frequency. The airfoil was drilled with through the median span. The pressure differences around the airfoil at different angles of attack were measured by using the Digital Manometer. The lift and drag coefficients ( $C_l$  and  $C_d$ ) were determined by numerically integrating the pressure distribution around the airfoil. Figure 4.4(a to d) shows the experimental setup used in the present study for the pressure difference measurement. During the experiment, the test airfoil was installed in the middle of the test section.

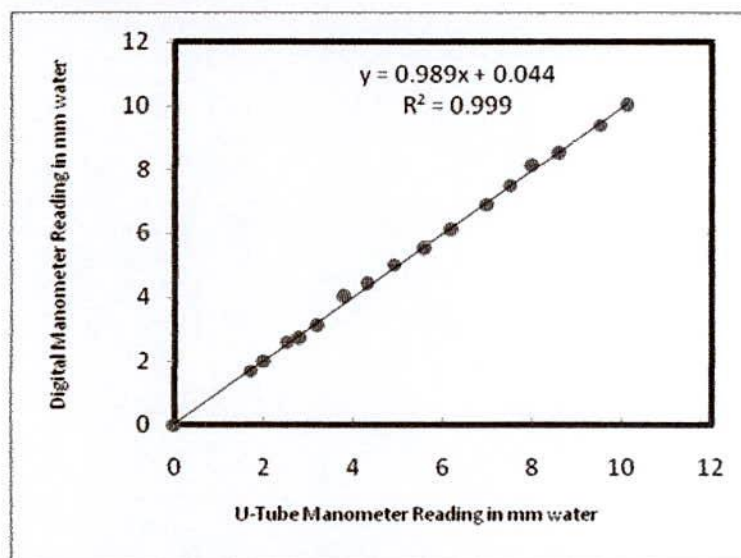


Figure 4.4(A): Calibration Curve of Digital Manometer

Digital Manometer is calibrated with the U-tube manometer and calibration curve is shown in Fig 4.4(A).



## CHAPTER V

### RESULTS AND DISCUSSION

#### 5.1 Motivation

After a century of theoretical research on the subject of airfoil and wing theory, the final word on the performance of an airfoil must still come from wind tunnel testing. The reason for this state of affairs is that the flow field around a wing is extremely complicated. The simplifying assumptions that are frequently introduced in order to treat the problem theoretically are much too severe to fail to influence the final results. Many of these assumptions are ignoring the effects of viscosity, nonlinearities in the equations of motion, three-dimensional effects, non-steady flow, free stream turbulence, and wing surface roughness. Nevertheless the theoretical prediction of lift produced by a wing has been reasonably successful (not quite so true for drag) and serves as an effective basis to study the experimental results.

When studying the flow about an airfoil it is best to begin with the simplest case, a flat plate. After understanding this case, it is possible to slowly work up the shape resembling a general airfoil, by gradually changing the shape of the flat plate and examining the flow about the body at each stage of change. Some of the important results of two-dimensional airfoil theory concerning  $C_l$  and  $C_m$  are shown in Fig 5.1(a), 5.1(b), 5.1(c), and 5.1(d). By definition:

Lift Coefficient: 
$$C_l = \frac{L}{\frac{1}{2} \rho_{\infty} U_{\infty}^2 c}$$

Pitching Moment Coefficient: 
$$C_m = \frac{M}{\frac{1}{2} \rho_{\infty} U_{\infty}^2 c^2}$$

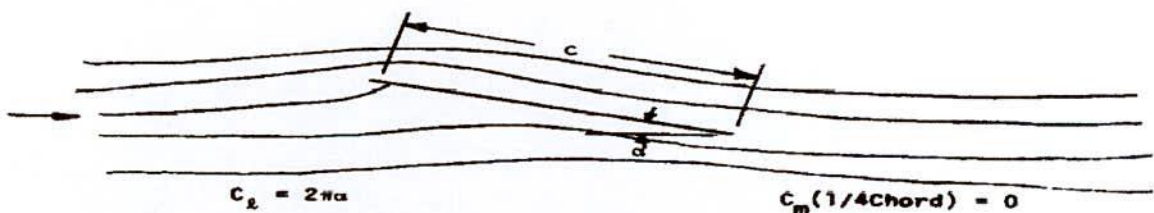


Figure 5.1(a): The flow around a flat plate placed in uniform flow.

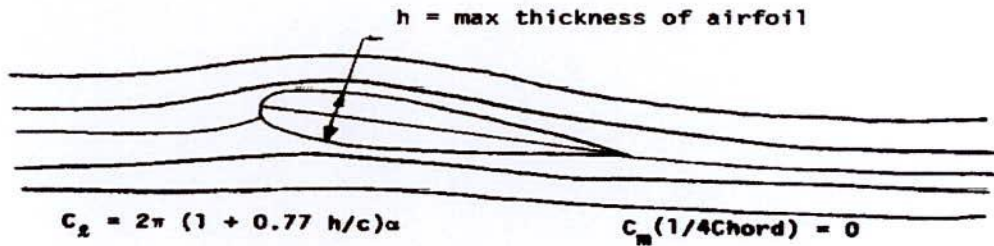


Figure 5.1(b): The flow around a Symmetric airfoil placed in uniform flow.

The effect of thickening the flat plate is to increase the lift curve slope  $dC_L/d\alpha$  slightly as can be seen from Fig 5.1(a) and Fig 5.1(b). However, this theoretical prediction is not observed experimentally, probably because of the viscous effects that are neglected in the inviscid theory. With respect to force and moment, the flat plate can be considered as a limiting case of a symmetric airfoil, as the ratio of thickness to chord approaches zero. Flow about a Circular Arc Airfoil is shown in Fig 5.1 (c).

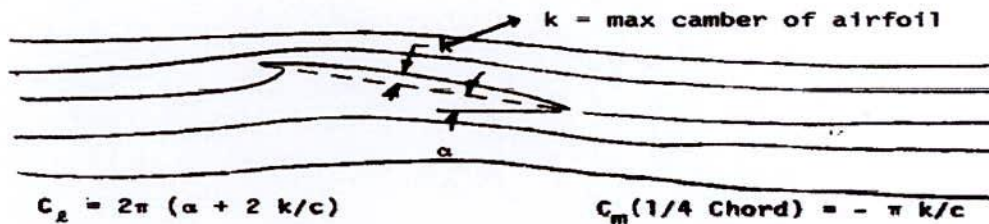


Figure 5.1(c): The flow around a Circular Arc Airfoil placed in uniform flow.

The effect of introducing circular-arc camber into the flat-plate airfoil is to decrease the angle of zero lift, i.e.,  $L = 0$  for  $\alpha = -2k/c$ . It also introduced a nose-down pitching moment about the 1/4 chord. The flow around a Joukowski Airfoil is depicted in Fig 5.1(d).

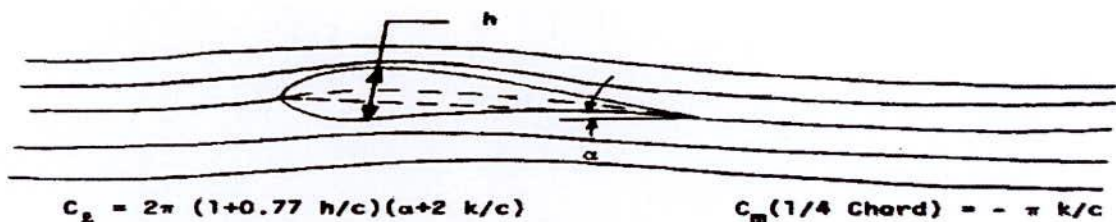


Figure 5.1(d): The flow around the General Joukowski Airfoil placed in uniform flow.

Although the Joukowski airfoil is a very special profile shape, the theoretical results are still useful in exhibiting the composite effect of thickness and camber.

## 5.2 Results and Discussion

### 5.2.1 Pressure Distribution

Frequency variation and pressure coefficients for the without control condition and test condition are shown in Fig. 5.2 (a) to 5.2 (i) for all measurement locations; corresponding no control and control contours are shown in Fig. 5.2 (j) and 5.2 (k) for lift and drag co-efficient respectively. Data at the test condition are shown here in dimensionless form according to eqns. 3.1, 3.2 and 3.3. The effect of the pressure coefficient on the upstream of the slot is considerable. Downstream of the slot, the separation point is not significantly affected but the pressure in the vicinity of separation reduces. Just downstream of separation, there is a relatively sharp pressure drop, followed by a pressure recovery that crosses over the no control line with reattachment occurring further upstream. This results in a curious situation where control appears to promote separation close to the control location while simultaneously shortening the reattachment length. The pressure coefficient distributions around the airfoil NACA 2415 when the angle of attack changing from 0 degrees to 20 degrees. When the angle of attack is relatively small (i.e., < 8 degrees), the pressure near the nose of the NACA 2415 airfoil was found to decrease quickly along the upper surface of the airfoil, and reached its negative pressure coefficient peak rapidly, then, the static pressure was found to recover over the upper surface of the airfoil gradually and smoothly up to the trailing edge of the airfoil, which is a typical behavior of the static pressure distribution over the upper surface of an airfoil without any flow separation. Over the separated region, the turbulent pressure fluctuations associated with control are significantly larger than those of the no control case. It is interesting to note that fluctuating turbulence peaks occur slightly upstream of reattachment for both the no control and control cases. The coherent fluctuations peak in the vicinity of  $C_{p,min}$  and then decay rapidly and approximately linearly, where the contributions of the coherent and turbulent fluctuations are almost same which has been shown Fig 5.2 (a) to 5.2 (d) . Thus, the region in which separation is promoted is

associated with amplification of the coherent pressure wave; the region of pressure recovery is associated with its dissipation.

As the angle of attack increased to  $8 \sim 10$  degrees, one distinctive characteristic of the pressure coefficient profiles along the upper surface of the airfoil is the region of nearly constant pressure (i.e., the "plateau" region) at  $0.08 < x/c < 0.2$ . Such "plateau" region in the pressure coefficient profiles would indicate the separation of the laminar boundary layer from the airfoil upper surface (i.e., flow separation occurred) [34]. The sudden increase in static pressure following the "plateau" serves to indicate the rapid transition of the separated laminar shear layer to turbulent flow, which would lead to the reattachment of the separated boundary layer and formation of a laminar separation bubble [35]. The static pressure profile was found to recover gradually and smoothly at downstream region of  $x/c > 0.25 \sim 0.30$ , which is as the same as those cases with smaller angle of attack and no flow separation. It indicates that the reattachment point, where the separated boundary layer reattach to the airfoil upper surface (i.e., the rear end of the separation bubble) would be located in the neighborhood of  $x/c \approx 0.25 \sim 0.30$  [36]. Generally the angle of attack becoming bigger than 12 degrees, the maximum absolute value of the pressure coefficient on airfoil upper surface near the leading edge was found to be only about 1.0, which is much smaller than that with smaller angle of attack (about 4.0). The static pressure over the entire upper surface of airfoil was found be nearly constant, i.e., the nearly constant pressure region was found to extend to the trailing edge of the airfoil, which indicates the separated shear layer fails to reattach to the airfoil upper surface, and flow separation would occur over entire upper surface of the airfoil [37], so the airfoil is found to stall completely as the angle of attack becoming greater than 12 degree. The experiment was carried out to observe the change in the coefficient of pressure of the upper surface of the airfoil in different angle of attack ( $\alpha$ ) and frequency (F) of suction and injection. It is seen from the Fig 5.2 (a) that, at angle of attack = 0 degree that, different absolute value of the pressure coefficient ( $C_p$ ) on airfoil upper surface was found for different frequency. In the graph shown in figure, for frequency  $F=2.0$ ,  $C_p$  is maximum (1) and for frequency  $F=1$ , the value is the lowest (0.5) up to chord length( $x/c$ )  $\approx 2.5$ . All other values are remaining within this range. And the pressure co-efficient ( $C_p$ ) nearly remained steady to the trailing edge of the airfoil as the  $x/c$  progress.

Figure 5.2 (b) shows that, for angle of attack,  $\alpha=2^\circ$  the maximum absolute value of the pressure coefficient on airfoil upper surface is maximum 1 (one) when  $x/c$  is 0.2 against all the frequencies respectively. The maximum lift increases for  $F=1.0$  which is 14% with respect to no control lift co-efficient. And it is decreasing gradually to the trailing edge of the airfoil. But  $C_p$  is increasing suddenly at the points ( $x/c=0.5, 6.5, 8, 9.5$ ) where suction and injection slot are considered as the  $x/c$  continues.

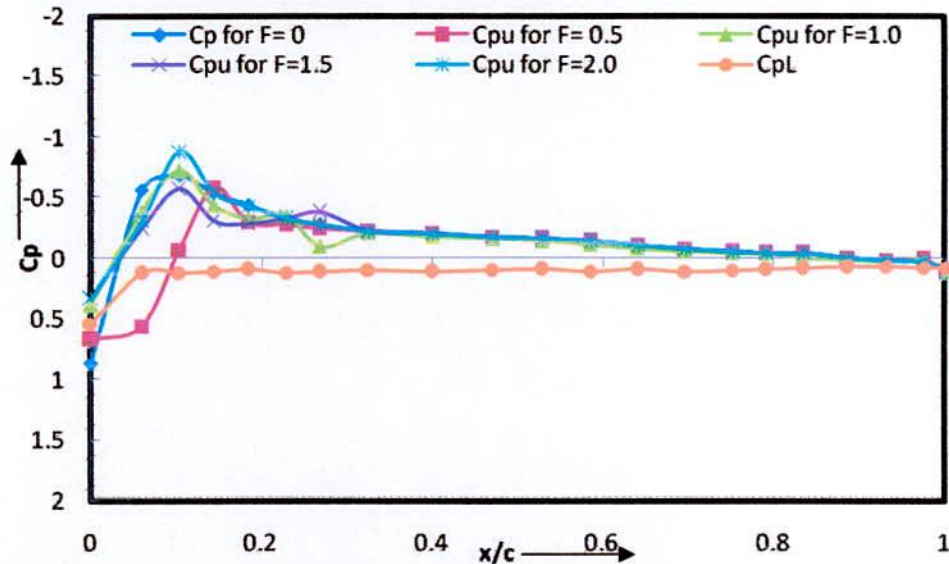


Figure 5.2(a): Pressure coefficient  $C_p$  distribution along the cord at  $\alpha = 0$  degree

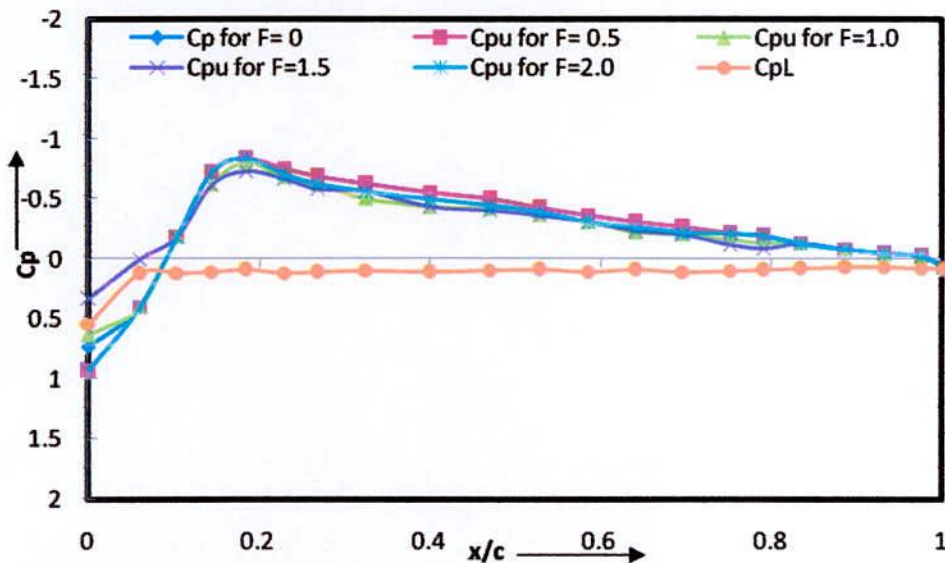


Figure 5.2(b): Pressure coefficient  $C_p$  distribution along the cord at  $\alpha = 2$  degree

Figure 5.2 (c) shows that, for  $\alpha= 4^\circ$  the maximum absolute value of the pressure coefficient on airfoil upper surface is maximum 1 (one) when  $x/c= 0.18$  to  $0.2$  against

all the frequencies respectively. It is almost similar to Fig 5.2 (b). Standard value of  $C_p$  nears same with the experimental value but here separation occurs slightly later. From the graph it is seen that no control curve declines before the peak point of all control curves.

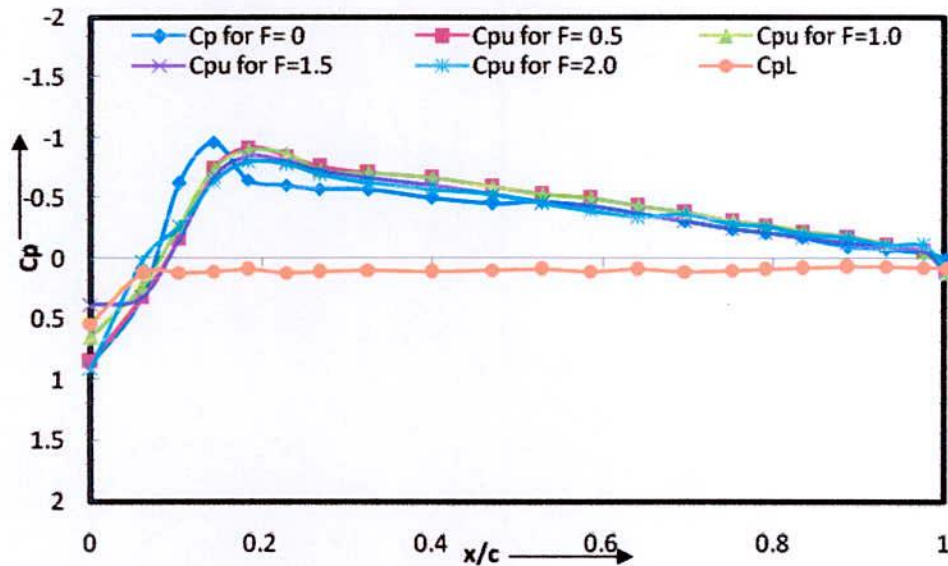


Figure 5.2(c): Pressure coefficient  $C_p$  distribution along the cord at  $\alpha = 4$  degree

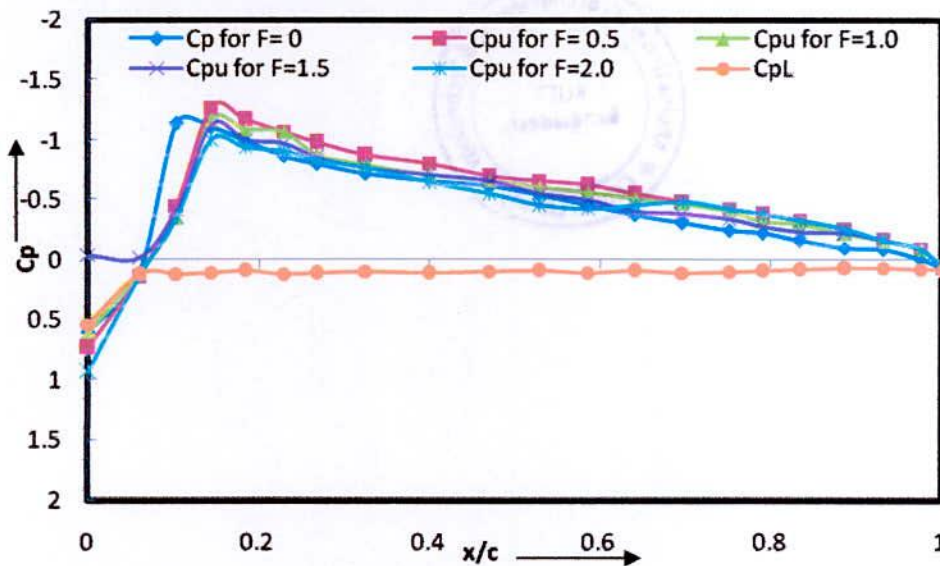


Figure 5.2(d): Pressure coefficient  $C_p$  distribution along the cord at  $\alpha = 6$  degree

These measurements illustrate to some degree the mechanism behind the observations discussed with respect to no control above: the blowing and suction phases tends to alternately promote and reduce separation close to the slot respectively. In a similar fashion, the near-wall velocity upstream of the slot alternately increases and decreases

depending on the phase. Fig 5.2 (d) shows that, for  $\alpha = 6$  degree, the maximum absolute value of the pressure coefficient on airfoil upper surface is maximum 1.4 when  $x/c$  is 0.15~0.2 against all the frequencies respectively. And it is decreasing gradually to the trailing edge of the airfoil with slight variation. It is significant that the variation of the curves due to angle change within 0-4 degree (Fig: 5.2 a to Fig: 5.2 c) is almost same but for 6 degree  $\alpha$  (Fig 5.2 d) the curve shows variation with each other for the change of frequency.

When the angle of attack increasing from 8 to 10 degrees, the measured surface pressure coefficient distributions given in Fig 5.2 e to 5.2 f revealed that a separation bubble would be generated on the upper surface of the airfoil at  $x/c \approx 0.15 \sim 0.25$ . Here the maximum absolute value of the pressure coefficient on the upper surface of airfoil increases up to 1.5. It is also observed that the flow reattaches where the slot ( $x/c \approx 0.5, 0.65, 0.8 \& 0.95$ ) is placed and the absolute value of pressure coefficient increases. As a consequence the lift force increases with decreasing the drag force. It is noticeable that the reattachment is greater at  $x/c \approx 0.5$  than at  $x/c \approx 0.95$ . it is shows from Fig 5.2 (e) that the maximum absolute pressure co-efficient( $C_p$ ) always greater than standard values of  $C_p$  and also shows that separation occur quickly as compared with standard curve. For no control curve the separation occurs after 10 %of total chord length but for control curve separation appears after 20% of chord length. At 8 degree angle of attack lift co-efficient increases 13.98% with respect to no control curve.

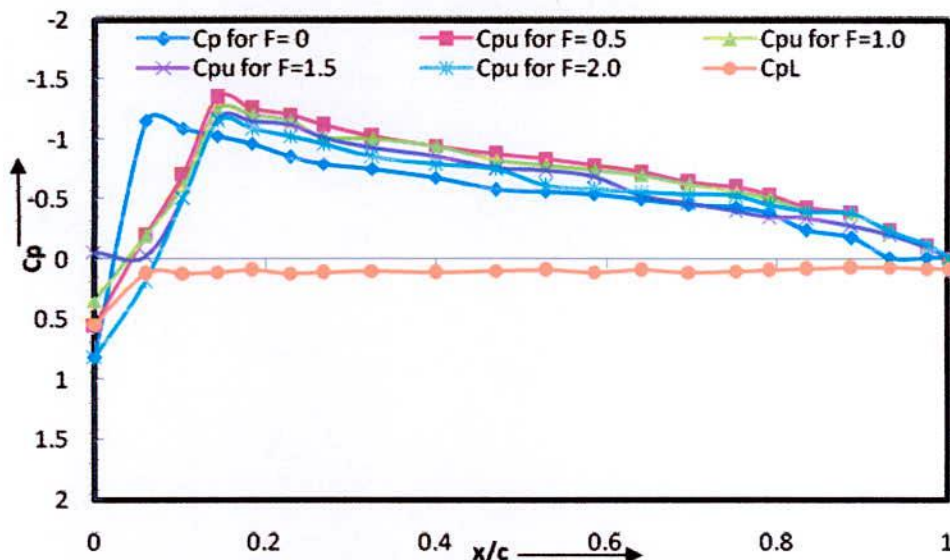


Figure 5.2(e): Pressure coefficient  $C_p$  distribution along the cord at  $\alpha = 8$  degree

Figure 5.2 (f) again shows that the magnitude of standard  $C_p$  (maximum 1.63 at  $x/c = .059$ ) is greater as compared with experimental value but it decreases quickly that means flow separated from the upper surface rapidly. On the other hand both Fig- 5.2 (e) and 5.2 (f) shows the average experimental value of  $C_p$  always greater than standard value that means the flow separation is reduces on the upper surface of airfoil. Also mention that flow is fully separated for standard value at  $x/c = 0.8$  but after using the said controlling method delay the separation of flow. At  $\alpha = 10$  degree the no control curve ( $F=0$ ) the co-efficient pressure curve the point is much greater than control curve and it begins earlier. Beside this the separation of no control curve reduces quickly and after 80% of  $x/c$  it detaches completely.

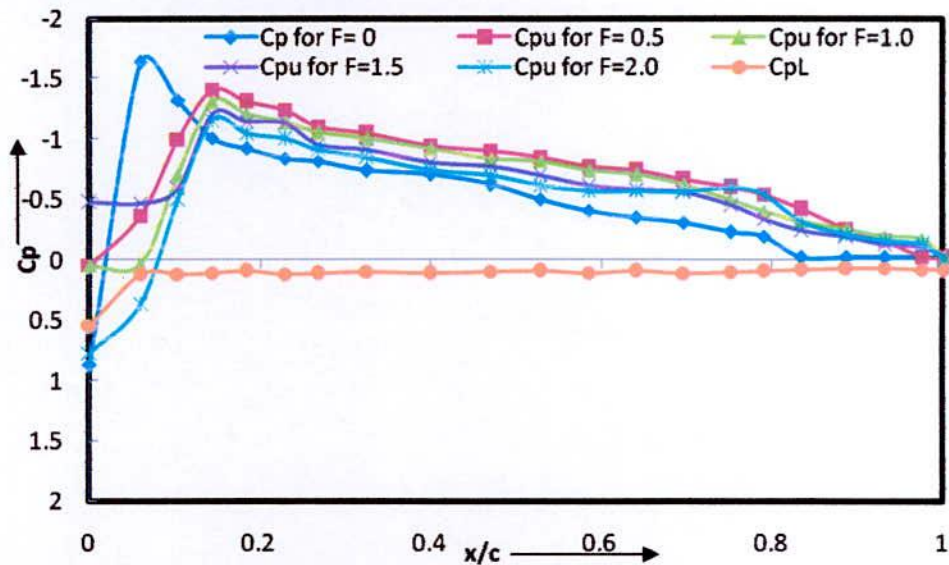


Figure 5.2(f): Pressure coefficient  $C_p$  distribution along the cord at  $\alpha = 10$  degree



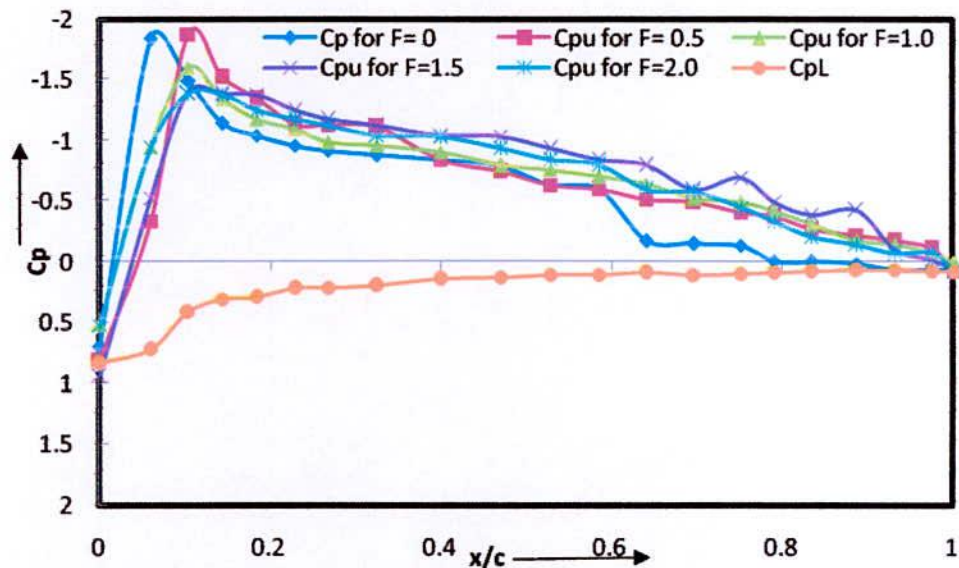


Figure 5.2(g): Pressure coefficient  $C_p$  distribution along the cord at  $\alpha=12$  degree

The angle of attack increasing to 12 degrees, the measured surface pressure coefficient distributions given in Fig 5.2 (g) found that a separation bubble would be generated on the upper surface of the airfoil at  $x/c \approx 0.10 \sim 0.20$ . From the figure it is seen that the maximum is gained  $C_p$  for control curve ( $F=0.5$ ). No control curve almost detaches after 60% of  $x/c$  and for control curves the pressure co-efficient is obtained until the trail edge. Here the maximum absolute value of the pressure coefficient on the upper surface of airfoil increases up to 1.86 at  $x/c = 0.1$ . The curve of  $C_p$  is almost straight line for all the frequencies but the standard value of  $C_p$  decrease gradually up to  $x/c = 0.65$  and then fluid flow fully separated. It is also observed that the flow reattaches where the slot ( $x/c \approx 0.5, 0.65, 0.8$ ) is placed and the absolute value of pressure coefficient increases. As a consequence the lift force increases with decreasing the drag force. But the reattachment of the flow after  $x/c \approx 0.8$  is not so remarkable.

The angle of attack increasing to 12 degrees, the measured surface pressure coefficient distributions given in Fig 5.2 (h) shown that a separation bubble would be generated on the upper surface of the airfoil at  $x/c \approx 0.05 \sim 0.15$ . Here the maximum absolute value of the pressure coefficient on the upper surface of airfoil increases up to 2.18. It is observed that the maximum elevation of  $C_p$  with compared all of other fig of  $C_p$ . For no control curve the  $C_p$  falls rapidly at  $x/c=40\%$  and for control curve at  $x/c=50\%$ . Because

due to increase in  $\alpha$  separation occurs prematurely at leading edge and greater lift force obtained for control curve.

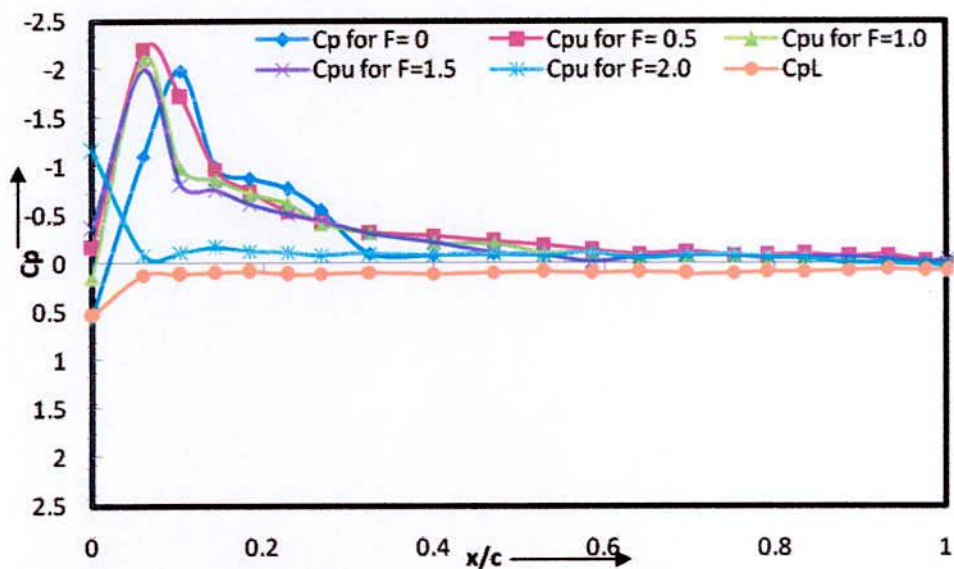


Figure 5.2(h): Pressure coefficient  $C_p$  distribution along the cord at  $\alpha = 14$  degree

It is seen from the Fig 5.2 (i) that, at  $\alpha= 20$  degree that, different absolute value of the pressure coefficient ( $C_p$ ) on airfoil upper surface was found for different frequency. The trend for all the frequency almost same but still some lift is found here. In the graph shown below, for high frequency  $F=2.0$ ,  $C_p$  is maximum (0.4) and almost same for all other frequency.

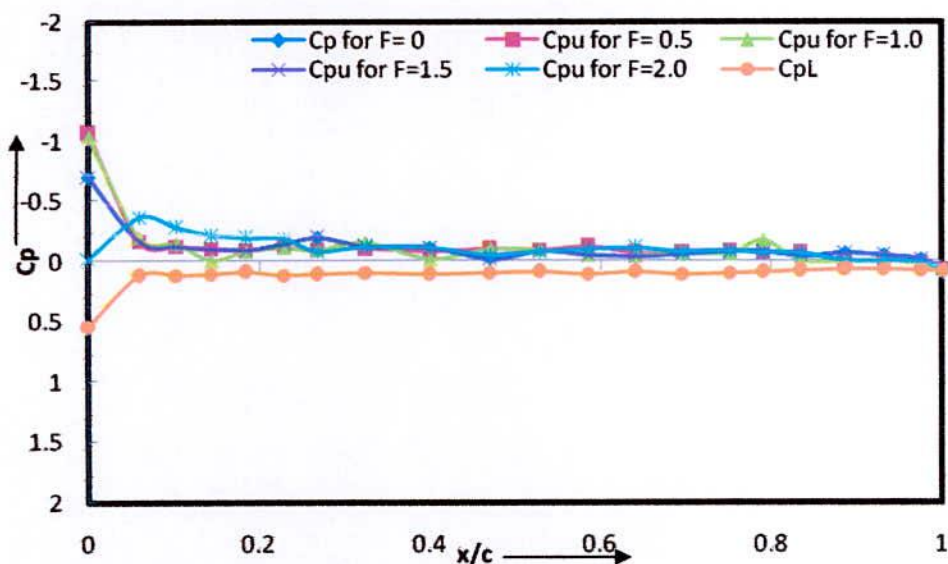
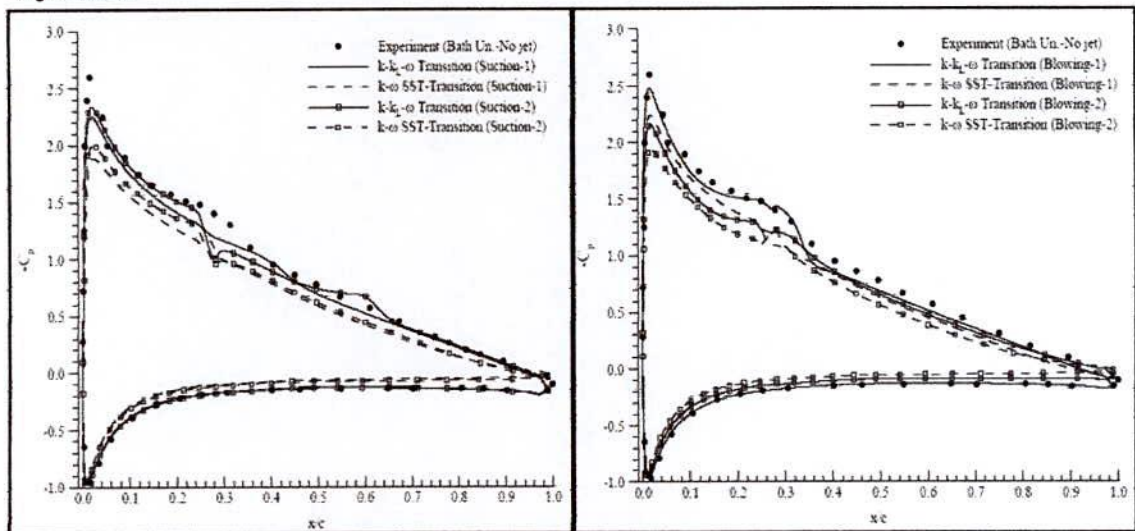


Figure 5.2(i): Pressure coefficient  $C_p$  distribution along the cord at  $\alpha = 20$  degree

The adverse pressure gradient over the upper surface of the airfoil would become bigger and bigger as the angle of attack increases. The measured surface pressure coefficient distributions given in Fig. 5.2 revealed that the separated shear layer would be able to reattach to the upper surface of the airfoil when the angle of attack increase up to 12 degrees and the airfoil would not stall completely due to the change pressure coefficient. Angle of attack,  $\alpha=12$  degrees is a high lift condition in take-off or landing. The lift coefficient in this angle of attack is increased by 4% due to surface suction and injection. Applying flow separation control technique like suction and injection by a slot than the separated shear layer would be able to reattach to the upper surface of the airfoil.

Unfortunately, no experimental works with suction and injection for this aerofoil is in author's knowledge. But numerical works have been done such as by Serdar et al. [38] and the result is that the suppression of the separation bubble and the reduction of the upper surface pressure coefficients increase the lift and decrease the drag. Figure 5.2 shows the pressure distribution over the NACA 2415 aerofoil simultaneous suction and injection.



(A)

(B)

Figure 5.2: Comparison of the experimental pressure distribution (No jet) over the NACA 2415 aerofoil and the numerical pressure distributions by (A) suction (B) injection.

From this experiment it is seen that the nature of pressure distribution curve competitively is in agreement with published paper for the same model.

Lift coefficients were calculated by integrating the pressures over the upper pressure sides of the wing. The results are shown in the form of  $C_l$  vs  $\alpha$  in the Fig 5.2(j) for the four values of frequency. For all frequency the nature of the lift curve is almost similar. From the figure it has been seen that the lift co-efficient increases with increasing  $\alpha$  and after certain time lift co-efficient decreases with increasing  $\alpha$ . The lift co-efficient curve is almost straight line for each frequency up to 6 degree  $\alpha$ . Here flow is fully attached with wing surface. After 6 degree  $\alpha$  a slight deflection is created and again increases lift co-efficient rapidly and reach it's maximum point at surrounding 12 degree angle of attack. After the maximum point of lift co-efficient at  $\alpha= 12$  degree, the values of  $C_l$  get decreasing. The point from which the value starts to decrease is called stall. The separation of the boundary layer explains why aircraft wings will abruptly lose lift at high inclination to the flow. This condition is called a stall. After stall point a dead flow region is created and flow is unable to re-attach with wing surface. Here flow is separated from the upper pressure surface. As a result the static pressure is started to increase drag force and decrease lift force. The increasing rate of lift co-efficient is higher from  $\alpha= 8$  to 14 degrees than from  $\alpha= 0$  to 6 degree. It is clearly said that by using flow separation control by suction and injection, fluid flow is re-attached from  $\alpha= 8$  to 14 degree and thus lift co-efficient is increased. In case of no control curve (Fig: 5.2 j) the lift co efficient is lower that the other control curves and the lift efficient curve is continuously increasing with increase of frequency. For maximum frequency ( $F=2$ ) lift is maximum but after pick point it reduces dramatically due to the higher  $\alpha$  and frequency the flow separation occurs rapidly.

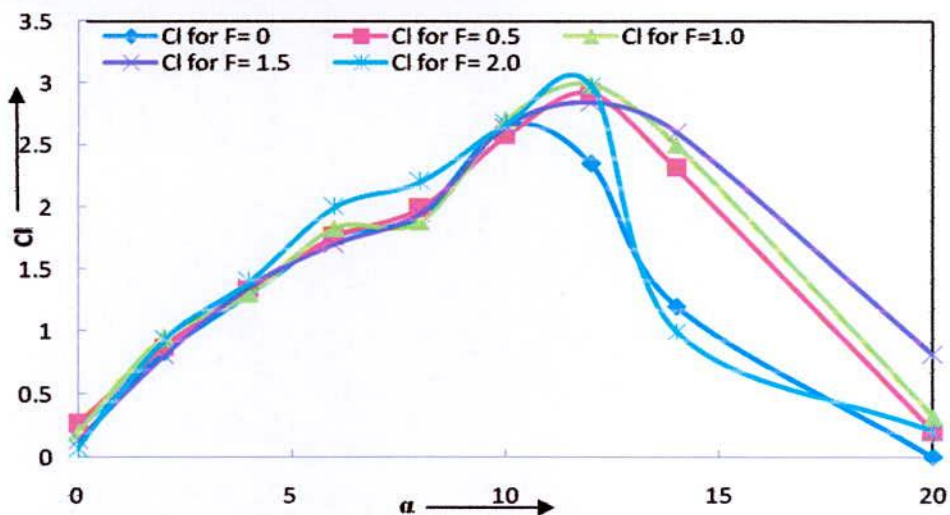


Figure 5.2 (j): Lift Coefficient  $C_l$  vs  $\alpha$

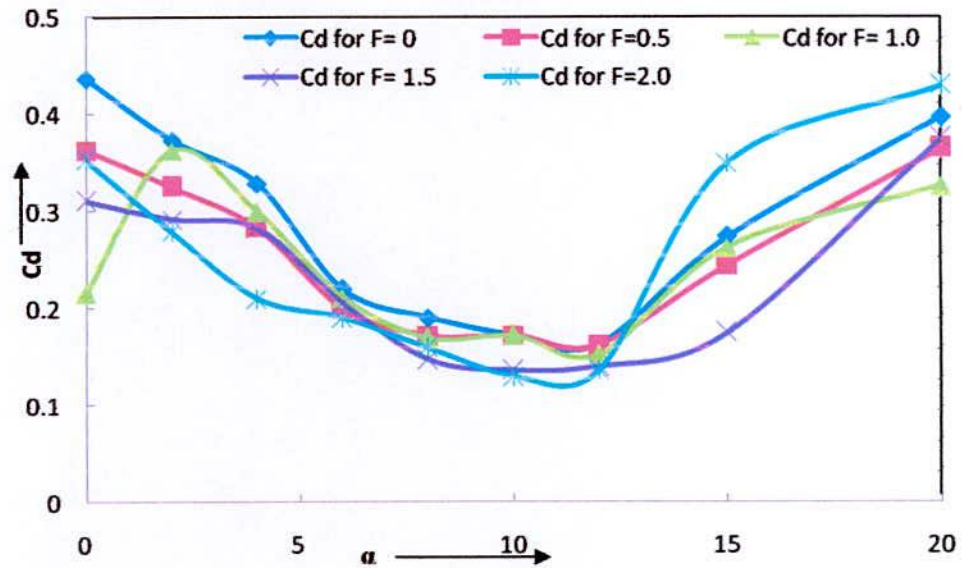


Figure 5.2 (k): Drag Coefficient  $C_d$  vs  $\alpha$

Similarly drag coefficients were calculated by integrating the pressures over the upper pressure sides of the wing. The results are shown in the form of  $C_d$  vs  $\alpha$  in the Fig 5.2 (k) for the four values of frequency. For all frequency the drag curves are near similar to each other. From the figure it has been seen that the drag co-efficient starts from about 3.5 with 0 degree  $\alpha$  and decreases with increasing  $\alpha$ . The drag co-efficient curve is decreased for each frequency up to 14 degree  $\alpha$  and then the value of  $C_d$  reaches lowest point. After this point flow is separated from the upper surface and creates a vortex. Consequently static pressure and drag force are increased with the decrease of lift force. Here flow is fully separated from wing surface. It is observed finally from the Fig 5.2 (j) and 5.2 (k) that the curve for standard value of  $C_l$  against  $\alpha$  is always lower than other curve and the curve for standard value of  $C_d$  against  $\alpha$  is always upper than other curve respectively. It is mention that from above both figs the lift co- efficient is increases with  $\alpha$  higher than the standard lift co- efficient and drag co- efficient is decreases with  $\alpha$  higher than the standard drag co-efficient. From Fig: 5.2 (j) it was seen that the maximum  $C_l$  lift co-efficient is obtained at  $\alpha= 14$  degree, simultaneously significant amount of drag reduction is observed. Due to this condition it can be said that it follows energy conservation law.

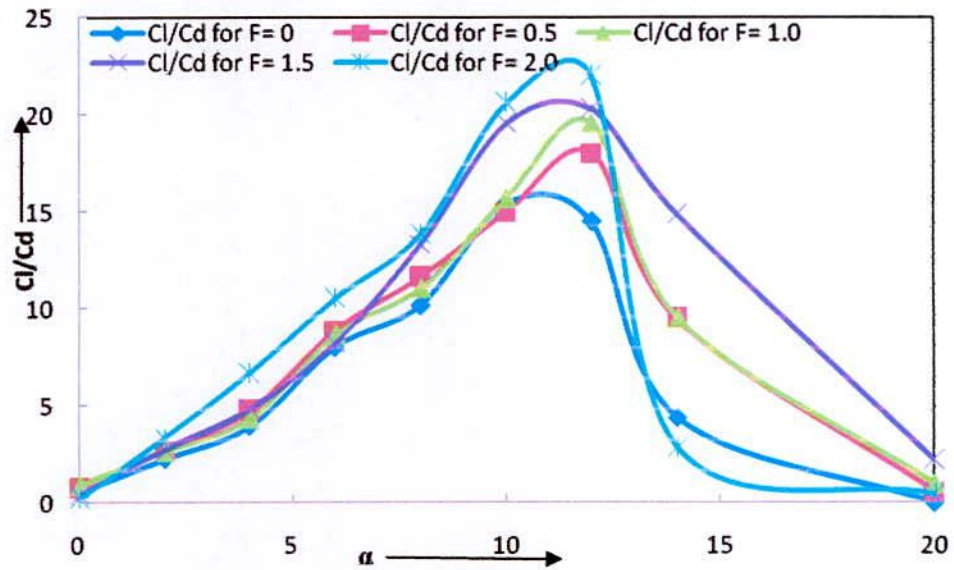


Figure 5.2 (l): Lift and Drag ratio vs  $\alpha$

Lift and drag are both aerodynamic forces, the ratio of lift to drag is an indication of the aerodynamic efficiency of the airplane. Aerodynamicists call the lift to drag ratio the L/D ratio, pronounced "L over D ratio." the L/D ratio is also equal to the ratio of the lift and drag coefficients. An airplane has a high L/D ratio if it produces a large amount of lift or a small amount of drag. Under cruise conditions lift is equal to weight. A high lift aircraft can carry a large payload. Under cruise conditions thrust is equal to drag. A low drag aircraft requires low thrust. Thrust is produced by burning a fuel and a low thrust aircraft requires small amounts of fuel be burned. Low fuel usage allows an aircraft to stay aloft for a long time, and that means the aircraft can fly long range missions. So an aircraft with a high L/D ratio can carry a large payload, for a long time, over a long distance. Fig 5.2 (l) shows that lifts and drag ratio Vs  $\alpha$  with varying suction and injection frequency. It was seen from the Fig 5.2 (j) lift is maximum but after pick point it reduces dramatically due to the higher  $\alpha$  and frequency the flow separation occurs rapidly the same phenomenon is observed in the fig 5.2 (l). From graph the L/D ratio increases sharply with increasing  $\alpha$  up to 12 degree and further increasing  $\alpha$  decrease L/D ration. It is also shown that the increase of L/D ratio increases the value of frequency of suction and injection. It found from the graph that the maximum value about 22 of L/D ratio is got in 12 degree angle of attack in frequency F=2.0. It is also observed that L/D ratio is increase for all the frequencies compared to standard value. For high frequency lift is rashes maximum but after pick point it reduce rapidly. From

other observation of pressure distribution curves that, always optimum lift is found for low frequency.

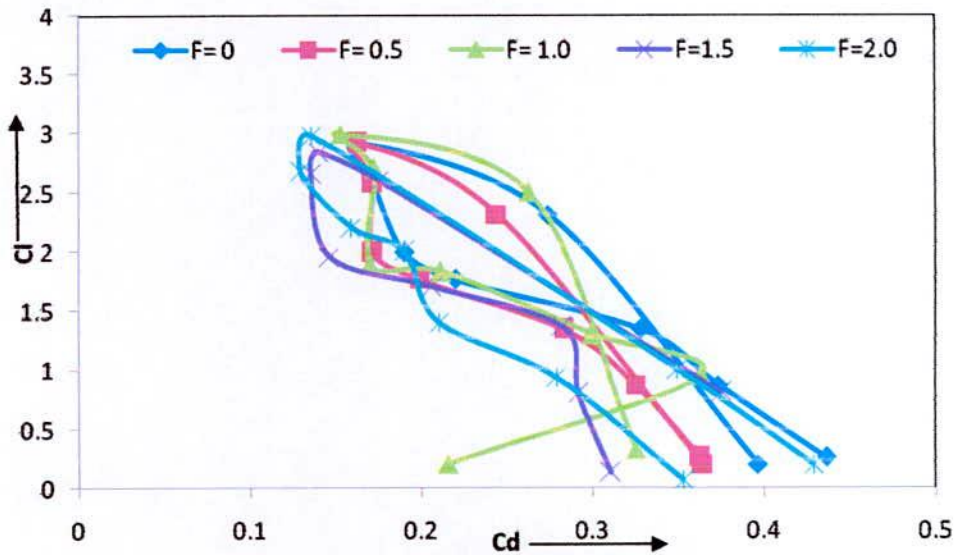


Figure 5.2(m): Coefficient of Lift vs Drag curve

The pattern of lift and drag curve with respect to angle of attack is describe in Fig5.2 (j) and Fig 5.2 (k). As discussed on the maximum flight time page, lift co-efficient increases with the increase of  $\alpha$  up to stall point and drag co-efficient decreases with increase of  $\alpha$  up to stall and after stall happens vice-versa. These characteristics are again shown in Fig 5.2(m), where the lift co-efficient increases sharply with the decrease of drag co-efficient to certain point and then a decrease of lift co-efficient with the increase of drag co-efficient is found. It is also seen from this figure that no control curve shows lower than the control curve. The boundary layer is mostly turbulent on such airplanes. Turbulent boundary layer has more surface friction than laminar boundary layer because when the flow is laminar, then fluid flow is attached with wing surface and the surface friction is lower. Again when the flow is turbulent, then fluid flow is separated from wing surface and a dead flow region is formed. As a result the surface friction is higher. Also, the separation of the boundary layer is associated with large energy losses and in most applications adversely affects the aerodynamic loads in the form of lift loss and drag increase. So it can be said that, the drag force is converted to lift force until the fluid flow remains attached with wing surface and the lift force is converted to drag force from when the fluid flow starts separating from wing surface. Thus the law of energy conservation is fully satisfied. Therefore, there is a strong tendency to delay or manipulate the occurrence of flow separation. Hence, separation

control is of great importance to most of the systems involving fluid flow, such as air, land or underwater vehicles and turbo machinery.

Lift coefficients were calculated by integrating the pressures over the suction and pressure sides of the wing. The results are shown in the graph of Fig 5.2 (a) to 5.2 (i) with respect to  $\alpha$ , for the four values of frequency. The benefit on the lift coefficient is large in the post stall area although it is reduced as is increased as seen in the last column, which is a comparison between the standard case and the present experimental case with the highest  $C_l$ . One of the reasons for this is that there were limitations in the actual position of slots. This suggests that even if it is find out that the optimization position of slot then some enhances increase the lift.

Table 5.1 Lift Co-efficient  $C_l$  for different frequencies.

$\alpha$	$C_l$ for F= 0	$C_l$ for F=0.5	$C_l$ for F= 1.0	$C_l$ for F= 1.5	$C_l$ for F= 2.0	Maximum $C_l$ Increase %
0	0.22	0.26	0.2	0.13	0.07	18.18182
2	0.83	0.87	0.95	0.8	0.93	14.45783
4	1.3	1.34	1.3	1.36	1.4	7.692308
6	1.76	1.76	1.83	1.7	2	3.977273
8	1.93	1.99	1.88	1.95	2.2	13.98964
10	2.5	2.57	2.7	2.65	2.67	6.8
12	2.85	2.92	2.99	2.84	2.98	4.912281
14	2.2	2.31	2.5	2.6	1	18.18182
20	0	0.2	0.32	0.81	0.2	-----

Drag co-efficient were calculated by the same procedure as lift co-efficient. The results are shown in the graph of Fig 5.2(k) with respect to angle of attack, for the four values of frequency. Here again table 5.2 again present data of drag co-efficient and comparison between the standard case and the present experimental case with the highest  $C_d$ .



Table 5.2 Drag Co-efficient  $C_d$  for different frequencies.

$\alpha$	$C_d$ for $F=0.0$	$C_d$ for $F=0.5$	$C_d$ for $F=1.0$	$C_d$ for $F=1.5$	$C_d$ for $F=2.0$	Maximum $C_d$ Decrease %
0	0.436256	0.362564	0.215832	0.310626	0.352564	50.52627
2	0.37325	0.324991	0.362564	0.29151	0.279144	25.21247
4	0.328311	0.283111	0.299144	0.282151	0.210072	36.01428
6	0.219905	0.199052	0.211072	0.20579	0.189905	13.64224
8	0.190141	0.17159	0.169905	0.146451	0.159014	22.9776
10	0.171794	0.171794	0.172159	0.135597	0.129718	24.49212
12	0.162286	0.162286	0.152718	0.140056	0.135623	16.42967
14	0.273931	0.243931	0.262286	0.174921	0.349309	36.1441
20	0.396439	0.364393	0.325362	0.374921	0.428641	17.92885

The adverse pressure gradient on the upper surface of the airfoil would become more severe as the angle of attack increasing. Since the laminar boundary layer is unable to withstand any significant adverse pressure gradient, it would separate from the upper surface of the airfoil, and laminar flow separation would occur as the angle of attack becoming bigger than 8 degrees. The separated laminar boundary layer would transit to turbulent flow rapidly by generating unsteady Kelvin-Helmholtz vortex structures, and the turbulent flow could reattach to the upper surface of the airfoil as a turbulent boundary by forming a separation bubble on the airfoil. Since the reattached turbulent boundary could attach to the upper surface of the airfoil firmly from the reattachment point up to the airfoil trailing edge, the lift coefficient of the airfoil was found to keep on increasing with the increasing angle of attack. However, the increase rate was found to slow down due to the formation of the separation bubble. The drag coefficient of the airfoil was also found to increase slightly with the increasing angle of attack. In this tunnel, our model arrangement corresponds to a blockage coefficient 2.2% for an angle of attack of 20 degrees. These tests can therefore simulate well the case of a wing in an infinite domain. The model was equipped with flat end plates to reduce as much as possible the end effects.

The effects of suction and injection on aerodynamic characteristics are investigated of an airfoil NACA 2415. To investigate the effect of suction and injection, the results are compared with the standard case. The following characteristics are compared for three

cases: lift coefficient and pressure drag coefficient. The most significant effect is in the lift. The results of lift coefficients for three cases are shown in Fig. 5.2 (j). In normal flight conditions, angle of attack of 6 and 10, a significant increase in lift coefficient equal to 4% and 7%, respectively. Angle of attack of 14 degrees is a high lift condition in take-off or landing. The lift coefficient in this angle of attack is increased by 18.18% due to surface suction and injection. In angle of attack of 20 degrees the increase in lift coefficient is 5.5%.

Fig 5.2(i) shows the pressure coefficient over the suction and injection side of the airfoil in angle of attack of 20 degrees. Although the slots are placed near the trailing edge, they affect the upstream flow. So the total pressure over the airfoil surface is affected by the suction and injection. The slots are actually sucking inside a reversed flow, which can somehow reduce the back-flow stream but cannot reverse the boundary layer Profile. The region that is actually involved in suction/injection process is the boundary layer.

To explain the effects of suction and injection as mentioned above, we take a closer look at the boundary layer profiles. Injection has an unwanted effect on lift coefficient. It dramatically lowers the lift coefficient. Injection lowers the surface friction coefficient while decreasing the lift coefficient. Injection can be employed when lowering the surface friction is more important than increasing the lift. An engineering compromise is needed to choose the right wall treatment to reach the desired goal. When the air is sucked into the wall the closest molecules and eddies to the wall are sucked in. It is obvious that the closest to the wall are the slowest. Therefore suction grabs the particles with minimum speed and the resulting profile lacks the low velocity particles in the bottom. It means that we artificially change the profile shape the way we desire. Exactly after the slot, the profile shape is sharper at the bottom. It means that the wall normal velocity gradient is higher and the shear stress is greater according to Stokes law. This results to higher skin friction. Under the influence of viscosity the boundary layer profile returns to its normal shape while the fluid travels on the solid surface. Before the second suction slot, the velocity profile is similar to the velocity profile before the first slot. The lower particles with greater velocity than what they have before give their energy to upper particles and the velocity profile is normalized again. The results show that the streamlines adjacent to solid are omitted from the field by being grabbed by the suction.

## CHAPTER VI

### CONCLUSIONS

#### 6.0 Conclusions

An experimental study has been accomplished to determine the effects of suction and injection in the aerodynamic characteristics of a specific airfoil NACA 2415. The purpose of this research was to develop a flow separation control mechanism that could generate secondary flow injection and suction by using single cylinder buster to increase the lift force of airfoils. It is concluded that the suction and injection can significantly increase the lift coefficient and decrease the skin friction. The design mechanism shows that uniform and more powerful secondary fluid flow could be generated along the slot of the airfoil. The frequency of the secondary fluid flow injection and suction was changed by changing the motor speed. The device is an excellent candidate to control flow separation, where the required frequency is changing with aircraft speed and angle of attack. As friction drag at the turbulent boundary layer is far greater than that at the laminar boundary layer, the basic idea of friction drag reduction is focused on delaying the occurrence of transition, expanding the range of laminar flow at the object surface, and reduces friction drag at the turbulent boundary layer. In the specific case studied here, at angle of attack ( $\alpha$ ) 8 degree, which is correspondent to normal flight conditions, suction and injection presents a significant increase in lift coefficient equal to 13.98% with respect to no control. Significant improvement was obtained in the lift coefficient for moderate to high angles of attack. But the effect decreases with the further increase of angle of attack, possibly due to less effective interaction between the disturbance and the shear layer.

## **Recommendations**

The future work is to determine the optimal injection and suction value related to Mach number and angle of attack. Also the optimal number of slots and the space between them is a case of further studies. Note that this work is accomplished by assuming the slots a simple opening on the airfoil surface. In the future studies variety of opening shapes can be studied in order to design a more efficient slot opening shape.

## References:

- [1] Prandtl, L. "Über Flüssigkeitsbewegung bei sehr kleiner Reibung", Proceedings, 3rd International Mathematics Congress, Heidelberg, Germany, pp. 484- 491, 1904.
- [2] Liu P. Q., Duan H. S. and He Y. W., "Numerical Study of Suction-Blowing Flow Control Technology for an Airfoil" , Journal of aircraft, Vol. 47, No. 1, January–February 2010.
- [3] Gad-el-Hak, M. (1996) "Compliant Coatings: a Progress Report," Appl. Mech. Rev. 49, no. 10, part 2, pp. S147-S157.
- [4] Braslow, A.L., 1999. A history of suction-type laminar-flow control with emphasis on flight research. American Institute of Aeronautics and Astronautics, Washington, D.C.
- [5] Barnwell, R.W. and M.Y. Hussaini, (Eds.), 1992. Natural Laminar Flow and Laminar Flow Control. Springer-Verlag, New York.
- [6] Bushnell, D.M., and Hefner, J.N. (editors) (1990) Viscous Drag Reduction in Boundary Layers, Progress in Astronautics and Aeronautics, vol. 123, American Institute of Aeronautics and Astronautics, Washington, D.C.
- [7] Cantwell, B.J. (1981) "Organized Motion in Turbulent Flow," Annu. Rev. Fluid Mech. 13, pp. 457-515.
- [8] Moin, P. and Bewley, T. (1994) "Feedback Control of Turbulence," Appl. Mech. Rev. 47, pp. S3-S13.
- [9] Gad-el-Hak, M. (1994) "Interactive Control of Turbulent Boundary Layers: A Futuristic Overview," AIAA J. 32, pp. 1753-1765.
- [10] Fiedler, H.E., and Fernholz, H.-H. (1990) "On Management and Control of Turbulent Shear Flows," Prog. Aerospace Sci. 27, pp. 305-387.
- [11] Choi, H., Moin, P., and Kim, J. (1994) "Active Turbulence Control for Drag Reduction in Wall- Bounded Flows," J. Fluid Mech. 262, pp. 75-110.
- [12] Fan, X., Hofmann, L., and Herbert, T. (1993) "Active Flow Control with Neural Networks," AIAA Paper No. 93-3273, Washington, D.C.
- [13] Jacobson, S.A., and Reynolds, W.C. (1995) "An Experimental Investigation towards the Active Control of Turbulent Boundary Layers," Department of Mechanical Engineering Report No. TF-64, Stanford University, Stanford, California.
- [14] Gad-el-Hak, M., and Blackwelder, R.F. (1989) "Selective Suction for Controlling Bursting Events in a Boundary Layer," AIAA J. 27, pp. 308-314

- [15] Abergel, F. and R. Temam, 1990. On some control problems in fluid mechanics. *Theor. Comput. Fluid Dyn.* 1: 303-325.
- [16] Choi, H., Temam, R., Moin, P., and Kim, J. (1993) "Feedback Control for Unsteady Flow and its Application to the Stochastic Burgers Equation," *J. Fluid Mech.* 253, pp. 509-543.
- [17] Gutmark, E., and Ho, C.-M. (1986) "Visualization of a Forced Elliptical Jet," *AIAA J.* 24, pp. 684-685.
- [18] Fiedler, H.E., Glezer, A., and Wignanski, I. (1988) "Control of Plane Mixing Layer: Some Novel Experiments," in *Current Trends in Turbulence Research*, eds. H. Branover, M. Mond and Y. Unger, *Progress in Astronautics and Aeronautics*, vol. 112, pp. 30-64, AIAA, Washington, D.C.
- [19] Fiedler, H.E., and Fernholz, H.-H. (1990) "On Management and Control of Turbulent Shear Flows," *Prog. Aerospace Sci.* 27, pp. 305-387.
- [20] Gutmark, E.J., Schadow, K.C., and Yu, K.H. (1995) "Mixing Enhancement in Supersonic Free Shear Flows," *Annu. Rev. Fluid Mech.* 27, pp. 375-417.
- [21] Viswanath, P.R. (1995) "Flow Management Techniques for Base and Afterbody Drag Reduction," *Prog. Aero. Sci.* 32, pp. 79-129
- [22] Gad-el-Hak, M. (1989) "Flow Control," *Appl. Mech. Rev.* 42, pp. 261-293.
- [23] Narasimha, R., and Sreenivasan, K.R. (1979) "Relaminarization of Fluid Flows," in *Advances in Applied Mechanics*, vol. 19, ed. C.-S. Yih, pp. 221-309, Academic Press, New York.
- [24] Thibert, J.J., Reneaux, J, and Schmitt, V. (1990) "ONERA Activities on Drag Reduction," *Proceedings of the Seventeenth Congress of the International Council of the Aeronautical Sciences*, vol. 1, pp. 1053-1064, Paper No. ICAS-90-3.6.1, American Institute of Aeronautics and Astronautics, Washington, D.C.
- [25] Wagner, R.D., M.C. Fischer, F.S. Collier Jr. and W. Pfenninger, 1990. Supersonic laminar flow control on commercial transports. *Proc. 17th Cong. of the Intl. Council of the Aeronaut. Sci.*, 1: 1073- 1089.
- [26] Barnwell, R.W., and Hussaini, M.Y. (editors) (1992) *Natural Laminar Flow and Laminar Flow Control*, Springer-Verlag, New York.
- [27] Gad-el-Hak, M., and Bushnell, D.M. (1991) "Separation Control: Review," *J. Fluids Eng.* 113, pp. 5-30.

- [28] Karim, M.A., and Acharya, M. (1994) "Control of the Dynamic-Stall Vortex over a Pitching Airfoil by Leading-Edge Suction," AIAA J. 32, pp. 1647-1655.
- [29] Alrefai, M., and Acharya, M. (1995) "Controlled Leading-Edge Suction for the Management of Unsteady Separation over Pitching Airfoils," AIAA Paper No. 95-2188, Washington, D.C.
- [30] Roos, F.W. (1996) ""Microblowing" for High-Angle-of-Attack Vortex Flow Control on a Fighter Aircraft," AIAA Paper No. 96-0543, Washington, D.C.
- [31] Schetz, J.A., 1984. Foundation of Boundary Layer Theory for Momentum, Heat and Mass Transfer. Prentice Hall.
- [32] William Rea and Alan Pope, Low Speed Wind Tunnel Testing, John Wiley and Sons, Toronto, 1984: 6
- [33] Rea and Pope, 10-11
- [34] Shum Y. K. and Marsden D. J., "Separation Bubble Model for Low Reynolds Number Airfoil Applications", Journal of Aircraft, Vol.31, No.4, 1994.
- [35] Yaruseych S., Sullivan P.E. and Kawall, J.G., "Coherent Structure in an Airfoil Boundary Layer and Wake at Low Reynolds Numbers", Physics of Fluids, Vol, 18, 044101, 2006.
- [36] Zifeng Yang, Fred L. Haan, Hu Hui and Hongwei Ma" An Experimental Investigation on the Flow Separation on aLow-Reynolds-Number Airfoil" AIAA-2007-0275.
- [37] Lin, J.C. M. and Pulley, L. L., "Low-Reynolds-Number Separation on an Airfoil", AIAA Journal, Vol.34, No. 8, 1996.
- [38] Serdar M. GENC and K. Unver "Control of Flow Separation and Transition Point over an Aerofoil at Low Re Number using Simultaneous Blowing and Suction" AIAA Journal, Vol.44, No. 5, 2010

**APPENDIX A**

Table-1: Averaged pressure distributions @  $\alpha=0$  degree

x/c	Angle of Attack 0 degree					CpL
	Cp @ F=0	Cpu @ F=.5	Cpu @ F= 1.0	Cpu @F=1.5	Cpu @ F=2	
0	0.867568	0.6756757	0.391891892	0.3378378	0.3378378	0.540541
0.059551	-0.56081	0.5608108	-0.385135135	-0.2432432	-0.3024324	0.128378
0.103747	-0.67568	-0.0675676	-0.716216216	-0.5675676	-0.8756757	0.121622
0.143747	-0.54358	-0.5810811	-0.431756757	-0.3040541	-0.5405405	0.108108
0.183747	-0.43297	-0.2972973	-0.324324324	-0.2837838	-0.4283784	0.094595
0.228489	-0.3277	-0.277027	-0.351351351	-0.3243243	-0.3243243	0.121622
0.267562	-0.27432	-0.2432432	-0.094594595	-0.3783784	-0.2783784	0.114865
0.32505	-0.22297	-0.222973	-0.202702703	-0.222973	-0.222973	0.101351
0.399547	-0.2027	-0.2027027	-0.175675676	-0.2027027	-0.2027027	0.114865
0.469958	-0.17568	-0.1756757	-0.155405405	-0.1756757	-0.1756757	0.101351
0.528239	-0.15541	-0.1554054	-0.135135135	-0.1554054	-0.1554054	0.094595
0.584934	-0.13514	-0.1351351	-0.108108108	-0.1351351	-0.1351351	0.108108
0.640838	-0.10811	-0.1081081	-0.081081081	-0.1081081	-0.1081081	0.094595
0.696741	-0.08108	-0.0810811	-0.054054054	-0.0810811	-0.0810811	0.108108
0.751693	-0.05405	-0.0540541	-0.040540541	-0.0540541	-0.0540541	0.101351
0.79043	-0.04054	-0.0405405	-0.040540541	-0.0405405	-0.0405405	0.094324
0.833726	-0.04054	-0.0405405	-0.006756757	-0.0405405	-0.0405405	0.084324
0.887252	-0.00676	-0.0067568	0.013513514	-0.0067568	-0.0067568	0.074324
0.931024	0.013514	0.0135135	0.033783784	0.0135135	0.0135135	0.067568
0.974919	0.012514	0.0125135	0.013513514	0.0337838	0.0337838	0.077568



Table-2: Averaged pressure distributions @  $\alpha=2$  degree

x/c	Angle of Attack 2 degree					CpL
	Cp @ F=0	Cpu @ F=.5	Cpu @ F= 1.0	Cpu @F=1.5	Cpu @ F=2	
0	0.739189	0.93918919	0.63918919	0.33918919	0.9391892	0.540541
0.05955	0.405405	0.40540541	0.40540541	0.00540541	0.4054054	0.128378
0.10375	-0.182432	-0.1824324	-0.1824324	-0.1824324	-0.1824324	0.121622
0.14375	-0.716216	-0.7162162	-0.6162162	-0.6162162	-0.7162162	0.108108
0.18375	-0.831081	-0.8310811	-0.8010811	-0.7310811	-0.8310811	0.094595
0.22849	-0.752703	-0.7527027	-0.6802703	-0.6702703	-0.7027027	0.121622
0.26756	-0.683784	-0.6837838	-0.6083784	-0.5837838	-0.6283784	0.114865
0.32505	-0.620811	-0.6208108	-0.5008108	-0.5608108	-0.5608108	0.101351
0.39955	-0.549324	-0.5493243	-0.4324324	-0.4324324	-0.4932432	0.114865
0.46996	-0.494595	-0.4945946	-0.4159459	-0.4045946	-0.4459459	0.101351
0.52824	-0.418919	-0.4189189	-0.3618919	-0.3618919	-0.3918919	0.094595
0.58493	-0.360541	-0.3605405	-0.3040541	-0.3040541	-0.3040541	0.108108
0.64084	-0.302703	-0.3027027	-0.2202703	-0.2302703	-0.2702703	0.094595
0.69674	-0.262973	-0.262973	-0.202973	-0.1972973	-0.222973	0.108108
0.75169	-0.209459	-0.2094595	-0.1609459	-0.1209459	-0.2094595	0.101351
0.79043	-0.189189	-0.1891892	-0.1291892	-0.0891892	-0.1891892	0.094324
0.83373	-0.128378	-0.1283784	-0.1283784	-0.1283784	-0.1283784	0.084324
0.88725	-0.081081	-0.0810811	-0.0810811	-0.0810811	-0.0810811	0.074324
0.93102	-0.040541	-0.0405405	-0.0405405	-0.0405405	-0.0405405	0.067568
0.97492	-0.02027	-0.0202703	-0.0202703	-0.0202703	-0.0202703	0.077568

Table-3: Averaged pressure distributions @  $\alpha=4$  degree

Angle of Attack 4 degree						
x/c	Cp @ F=0	Cpu @ F=.5	Cpu @ F= 1.0	Cpu @F=1.5	Cpu @ F=2	Cpl
0	0.885135	0.85135135	0.651351351	0.38513514	0.913513514	0.540541
0.059551	0.324324	0.32432432	0.243243243	0.32432432	0.024324324	0.128378
0.103747	-0.62162	-0.1621622	-0.262162162	-0.16216216	-0.262162162	0.121622
0.143747	-0.96074	-0.7364865	-0.736486486	-0.67364865	-0.636486486	0.108108
0.183747	-0.64892	-0.9189189	-0.891891892	-0.84891892	-0.801891892	0.094595
0.228489	-0.60446	-0.8445946	-0.864594595	-0.80445946	-0.784459459	0.121622
0.267562	-0.57268	-0.7567568	-0.726756757	-0.72675676	-0.701567568	0.114865
0.32505	-0.56703	-0.7027027	-0.702702703	-0.67027027	-0.627027027	0.101351
0.399547	-0.50216	-0.6621622	-0.662162162	-0.60216216	-0.566216216	0.114865
0.469958	-0.45278	-0.5878378	-0.587837838	-0.52783784	-0.528783784	0.101351
0.528239	-0.47027	-0.527027	-0.527027027	-0.47027027	-0.452702703	0.094595
0.584934	-0.43243	-0.4932432	-0.493243243	-0.43243243	-0.393243243	0.108108
0.640838	-0.37432	-0.4324324	-0.432432432	-0.37432432	-0.343243243	0.094595
0.696741	-0.30838	-0.3783784	-0.378378378	-0.30837838	-0.358378378	0.108108
0.751693	-0.24054	-0.3040541	-0.304054054	-0.24054054	-0.284054054	0.101351
0.79043	-0.2077	-0.277027	-0.277027027	-0.2077027	-0.267027027	0.094324
0.833726	-0.17297	-0.222973	-0.222972973	-0.17297297	-0.202297297	0.084324
0.887252	-0.09432	-0.1824324	-0.182432432	-0.12432432	-0.168243243	0.074324
0.931024	-0.08022	-0.1216216	-0.121621622	-0.10021622	-0.112162162	0.067568
0.974919	-0.04054	-0.0540541	-0.054054054	-0.05405405	-0.105405405	0.077568

Table-4: Averaged pressure distributions @  $\alpha = 6$  degree

x/c	Angle of Attack 6 Degree					
	Cp @ F=0	Cpu @ F=.5	Cpu @ F= 1.0	Cpu @F=1.5	Cpu @ F=2	CpL
0	0.603648649	0.7364865	0.6036486	-0.0364865	0.93648649	0.540541
0.059551	0.114189189	0.1418919	0.1141892	-0.0141892	0.14189189	0.128378
0.103747	-1.134594595	-0.4459459	-0.3459459	-0.4159459	-0.3459459	0.121622
0.143747	-1.102702703	-1.2702703	-1.1702703	-1.1302703	-1.0027027	0.108108
0.183747	-0.989189189	-1.1689189	-1.0891892	-1.0029189	-0.9400169	0.094595
0.228489	-0.867567568	-1.0675676	-1.0675676	-0.9756757	-0.9067568	0.121622
0.267562	-0.797297297	-0.9797297	-0.8797297	-0.850973	-0.837973	0.114865
0.32505	-0.716216216	-0.8716216	-0.7916216	-0.7680162	-0.7671622	0.101351
0.399547	-0.654054054	-0.8040541	-0.7054054	-0.7054054	-0.6405405	0.114865
0.469958	-0.609459459	-0.6959459	-0.6594595	-0.6594595	-0.5495946	0.101351
0.528239	-0.540540541	-0.6554054	-0.6054054	-0.5540541	-0.4554054	0.094595
0.584934	-0.456216216	-0.6216216	-0.5621622	-0.5021622	-0.4216216	0.108108
0.640838	-0.372972973	-0.5472973	-0.5072973	-0.4047297	-0.4547297	0.094595
0.696741	-0.304864865	-0.4864865	-0.4648649	-0.3864865	-0.4864865	0.108108
0.751693	-0.240067568	-0.4256757	-0.4006757	-0.3425676	-0.4256757	0.101351
0.79043	-0.218378378	-0.3783784	-0.3183784	-0.2783784	-0.3783784	0.094324
0.833726	-0.158108108	-0.3310811	-0.3010811	-0.2331081	-0.3310811	0.084324
0.887252	-0.100215676	-0.2567568	-0.2156757	-0.2256757	-0.2567568	0.074324
0.931024	-0.081554054	-0.1554054	-0.1554054	-0.1554054	-0.1554054	0.067568
0.974919	-0.005878378	-0.0878378	-0.0878378	-0.0878378	-0.0878378	0.077568



Table-5: Averaged pressure distributions @  $\alpha = 8$  degree

x/c	Angle of Attack $\alpha = 8$ degree					
	Cp @ F=0	Cpu @ F=.5	Cpu @ F= 1.0	Cpu @F=1.5	Cpu @ F=2	CpL
0	0.815540541	0.5540541	0.354054054	-0.05540541	0.81554054	0.540541
0.059551	-1.144594595	-0.1891892	-0.189189189	-0.01891892	0.18918919	0.128378
0.103747	-1.09	-0.7094595	-0.609459459	-0.50945946	-0.5094595	0.121622
0.143747	-1.027027027	-1.3445946	-1.244594595	-1.17459459	-1.1445946	0.108108
0.183747	-0.964864865	-1.25	-1.2	-1.15	-1.09	0.094595
0.228489	-0.852702703	-1.2027027	-1.15027027	-1.12027027	-1.027027	0.121622
0.267562	-0.793918919	-1.1148649	-1.014864865	-1.01148649	-0.9648649	0.114865
0.32505	-0.751621622	-1.0202703	-1.00027027	-0.9302027	-0.8527027	0.101351
0.399547	-0.678378378	-0.9391892	-0.939189189	-0.85939189	-0.7939189	0.114865
0.469958	-0.578378378	-0.8716216	-0.821621622	-0.75716216	-0.7516216	0.101351
0.528239	-0.55972973	-0.8378378	-0.778378378	-0.73783784	-0.6078378	0.094595
0.584934	-0.541891892	-0.7837838	-0.737837838	-0.68378378	-0.5783784	0.108108
0.640838	-0.501351351	-0.7297297	-0.697297297	-0.52972973	-0.5597297	0.094595
0.696741	-0.450405405	-0.6418919	-0.621891892	-0.46418919	-0.5418919	0.108108
0.751693	-0.430135135	-0.6013514	-0.560135135	-0.40135135	-0.5301351	0.101351
0.79043	-0.380405405	-0.5405405	-0.505405405	-0.35405405	-0.4504054	0.094324
0.833726	-0.240391892	-0.4391892	-0.401891892	-0.34391892	-0.4039189	0.084324
0.887252	-0.178378378	-0.3783784	-0.378378378	-0.27837838	-0.3783784	0.074324
0.931024	-0.012297297	-0.2297297	-0.22972973	-0.20297297	-0.2297297	0.067568
0.974919	-0.010021622	-0.1216216	-0.121621622	-0.10216216	-0.1216216	0.077568

Table-6: Averaged pressure distributions @  $\alpha = 10$  degree

x/c	Angle of Attack 10 degree					
	Cp @ F=0	Cpu @ F=.5	Cpu @ F= 1.	Cpu @F=1.5	Cpu @ F=2	CpL
0	0.872973	0.0472973	0.0472973	-0.472973	0.77297297	0.540541
0.059551	-1.63054	-0.364865	0.0364865	-0.4648649	0.36486486	0.128378
0.103747	-1.32041	-0.993243	-0.699324	-0.5932432	-0.4932432	0.121622
0.143747	-1.00649	-1.405405	-1.305405	-1.2054054	-1.1540541	0.108108
0.183747	-0.91392	-1.304054	-1.204054	-1.1405405	-1.0405405	0.094595
0.228489	-0.83865	-1.236486	-1.136486	-1.1236486	-1	0.121622
0.267562	-0.81446	-1.101351	-1.051351	-0.9513514	-0.9101351	0.114865
0.32505	-0.73703	-1.040541	-1.000541	-0.9054054	-0.8405405	0.101351
0.399547	-0.70365	-0.939189	-0.913919	-0.8059189	-0.7391892	0.114865
0.469958	-0.62162	-0.898649	-0.838649	-0.7698649	-0.6986486	0.101351
0.528239	-0.50135	-0.844595	-0.814459	-0.6945946	-0.6145946	0.094595
0.584934	-0.40541	-0.77027	-0.737027	-0.6127027	-0.5702703	0.108108
0.640838	-0.35189	-0.736486	-0.703649	-0.5848649	-0.5736486	0.094595
0.696741	-0.31257	-0.662162	-0.621622	-0.5621622	-0.5662162	0.108108
0.751693	-0.22919	-0.601351	-0.501351	-0.4601351	-0.6013514	0.101351
0.79043	-0.19568	-0.540541	-0.405405	-0.3405405	-0.5405405	0.094324
0.833726	-0.02027	-0.418919	-0.318919	-0.2418919	-0.3189189	0.084324
0.887252	-0.02027	-0.256757	-0.256757	-0.1875676	-0.2125676	0.074324
0.931024	-0.02027	-0.162162	-0.196216	-0.1321622	-0.1621622	0.067568
0.974919	-0.02027	-0.027027	-0.17027	-0.1027027	-0.127027	0.077568

Table-7: Averaged pressure distributions @  $\alpha = 12$  degree

x/c	Angle of Attack 12 degree					CpL
	Cp @ F=0	Cpu @ F=.5	Cpu @ F= 1	Cpu @F=1.5	Cpu @ F=2	
0	0.704054	0.8040541	0.5202703	0.94594595	0.52027	0.840541
0.059551	-1.83108	-0.3310811	-0.939189	-0.5202703	-0.939189	0.728378
0.103747	-1.48649	-1.8648649	-1.594595	-1.3918919	-1.378378	0.421622
0.143747	-1.13514	-1.5135135	-1.337838	-1.3783784	-1.371622	0.310811
0.183747	-1.03378	-1.3378378	-1.168919	-1.3716216	-1.243243	0.294595
0.228489	-0.9527	-1.127027	-1.087838	-1.2432432	-1.168919	0.221622
0.267562	-0.91216	-1.1216216	-0.97973	-1.1689189	-1.114865	0.214865
0.32505	-0.87162	-1.1062162	-0.952703	-1.1148649	-1.033784	0.201351
0.399547	-0.83108	-0.8310811	-0.898649	-1.0337838	-1.027027	0.148649
0.469958	-0.78378	-0.7378378	-0.790541	-1.027027	-0.925676	0.135135
0.528239	-0.62838	-0.6283784	-0.75	-0.9256757	-0.831081	0.109459
0.584934	-0.58784	-0.5878378	-0.695946	-0.8310811	-0.790541	0.108108
0.640838	-0.16892	-0.5068919	-0.635135	-0.7905405	-0.587838	0.094595
0.696741	-0.14865	-0.4864865	-0.52027	-0.5878378	-0.568919	0.108108
0.751693	-0.12838	-0.4012838	-0.485135	-0.6891892	-0.448649	0.101351
0.79043	-0.00676	-0.3675676	-0.412838	-0.4864865	-0.328378	0.094324
0.833726	0	-0.2675676	-0.306757	-0.3837838	-0.206757	0.084324
0.887252	0.013514	-0.2135135	-0.167568	-0.4200676	-0.135135	0.074324
0.931024	0.067568	-0.1675676	-0.135135	-0.1006757	-0.067568	0.067568
0.974919	0.067568	-0.1067568	-0.067568	-0.0135135	-0.077568	0.077568

Table-8: Averaged pressure distributions @  $\alpha = 14$  degree

x/c	Angle of Attack 14 degree					CpL
	Cp @ F=0	Cpu @ F=.5	Cpu @ F= 1.0	Cpu @F=1.5	Cpu @ F=2	
0	0.554054	-0.1554054	0.155405405	-0.3554054	-1.155405405	0.540541
0.059551	-1.09878	-2.1848784	-2.098783784	-1.9878378	-0.087837838	0.128378
0.103747	-1.98108	-1.7081081	-0.981081081	-0.8081081	-0.108108108	0.121622
0.143747	-0.98554	-0.9655405	-0.855405405	-0.7554054	-0.155405405	0.108108
0.183747	-0.87122	-0.7421622	-0.712162162	-0.6121622	-0.121621622	0.094595
0.228489	-0.76081	-0.5310811	-0.608108108	-0.5081081	-0.108108108	0.121622
0.267562	-0.54088	-0.4287838	-0.408783784	-0.4350878	-0.087837838	0.114865
0.32505	-0.10135	-0.3213514	-0.310135135	-0.3101351	-0.101351351	0.101351
0.399547	-0.08108	-0.2810811	-0.208108108	-0.2181081	-0.081081081	0.114865
0.469958	-0.09459	-0.2209459	-0.194594595	-0.1045946	-0.094594595	0.101351
0.528239	-0.08784	-0.1878378	-0.108783784	-0.0783784	-0.087837838	0.094595
0.584934	-0.11486	-0.1314865	-0.114864865	-0.0148649	-0.114864865	0.108108
0.640838	-0.06081	-0.1000811	-0.060810811	-0.0708108	-0.060810811	0.094595
0.696741	-0.08108	-0.1208108	-0.081081081	-0.0910811	-0.081081081	0.108108
0.751693	-0.08784	-0.0878378	-0.087837838	-0.0783784	-0.087837838	0.101351
0.79043	-0.06757	-0.0756757	-0.067567568	-0.0575676	-0.067567568	0.094324
0.833726	-0.06081	-0.0908108	-0.060810811	-0.0678108	-0.060810811	0.084324
0.887252	-0.00676	-0.0675676	-0.006756757	-0.0655676	-0.006756757	0.074324
0.931024	0	-0.082154	0	-0.04	0	0.067568
0.974919	0.013514	-0.0135135	0.013513514	-0.0135135	0.013513514	0.077568

Table-9: Averaged pressure distributions @  $\alpha = 20$  degree

x/c	Angle of Attack 20 degree					CpL
	Cp @ F=0	Cpu @ F=.5	Cpu @ F= 1.0	Cpu @F=1.5	Cpu @ F=2	
0	-0.70135	-1.0635135	-1.035135135	-0.7013514	-0.013513514	0.540541
0.059551	-0.16216	-0.1621622	-0.192162162	-0.1621622	-0.362162162	0.128378
0.103747	-0.12162	-0.1216216	-0.141621622	-0.1216216	-0.272162162	0.121622
0.143747	-0.10135	-0.1013514	-0.001351351	-0.1013514	-0.217351351	0.108108
0.183747	-0.08784	-0.0878378	-0.078378378	-0.0878378	-0.187837838	0.094595
0.228489	-0.13811	-0.1081081	-0.108108108	-0.1381081	-0.181081081	0.121622
0.267562	-0.18784	-0.0878378	-0.087837838	-0.1878378	-0.078378378	0.114865
0.32505	-0.12135	-0.1013514	-0.151351351	-0.1213514	-0.113513514	0.101351
0.399547	-0.10811	-0.0810811	-0.010810811	-0.1081081	-0.108108108	0.114865
0.469958	-0.00946	-0.0945946	-0.094594595	-0.0094595	-0.045945946	0.101351
0.528239	-0.07838	-0.0878378	-0.087837838	-0.0783784	-0.078378378	0.094595
0.584934	-0.04865	-0.1148649	-0.048648649	-0.0486486	-0.101486486	0.108108
0.640838	-0.03081	-0.0608108	-0.040810811	-0.0308108	-0.106081081	0.094595
0.696741	-0.05108	-0.0810811	-0.061081081	-0.0510811	-0.081081081	0.108108
0.751693	-0.07784	-0.0878378	-0.057837838	-0.0778378	-0.087837838	0.101351
0.79043	-0.07757	-0.0675676	-0.167567568	-0.0775676	-0.067567568	0.094324
0.833726	-0.04081	-0.0608108	-0.000810811	-0.0408108	-0.060810811	0.084324
0.887252	-0.06757	-0.0067568	0.006756757	-0.0675676	-0.006756757	0.074324
0.931024	-0.04162	0	0.002613	-0.04162	0	0.067568
0.974919	-0.01351	0.0135135	0.035135135	-0.0135135	0.013513514	0.077568



Table-10: Lift Co-efficient at different  $\alpha$ 

$\alpha$	Cl for F=0	Cl for F=.5	Cl for F=1	Cl for F=1.5	Cl for F=2
0	0.22	0.26	0.2	0.13	0.07
2	0.83	0.87	0.95	0.8	0.93
4	1.3	1.34	1.3	1.36	1.4
6	1.76	1.76	1.83	1.7	2
8	1.93	1.99	1.88	1.95	2.2
10	2.65	2.57	2.7	2.65	2.67
12	2.35	2.92	2.99	2.84	2.98
14	1.2	2.31	2.5	2.6	1
20	0	0.2	0.32	0.81	0.2

Table-11: Drag Co-efficient at different  $\alpha$ 

$\alpha$	Cd for F=0	Cd for F=0.5	Cd for F=1	Cd for F=1.5	Cd for F=2
0	0.436256	0.362564	0.215832	0.310626	0.352564
2	0.37325	0.324991	0.362564	0.29151	0.279144
4	0.328311	0.283111	0.299144	0.282151	0.210072
6	0.219905	0.199052	0.211072	0.20579	0.189905
8	0.190141	0.17159	0.169905	0.146451	0.159014
10	0.171794	0.171794	0.172159	0.135597	0.129718
12	0.162286	0.162286	0.152718	0.140056	0.135623
14	0.273931	0.243931	0.262286	0.174921	0.349309
20	0.396439	0.364393	0.325362	0.374921	0.428641

Table-12: Lift / Drag ratio at different  $\alpha$

$\alpha$	Cl/Cd,F=0	Cl/Cd,F=.5	Cl/Cd,F=1	Cl/Cd,F=1.5	Cl/Cd,F=2
0	0.504291	0.717115	0.926645	0.41851	0.198546
2	2.223711	2.676994	2.620227	2.744332	3.331609
4	3.959659	4.733131	4.345728	4.820113	6.664375
6	8.003447	8.841894	8.670019	8.260833	10.53157
8	10.15038	11.5974	11.06499	13.31504	13.83525
10	15.42546	14.95979	15.68318	19.54316	20.58312
12	14.48062	17.99294	19.57858	20.27765	21.9727
14	4.380667	9.469896	9.531584	14.86385	2.862796
20	0	0.548858	0.983519	2.160455	0.466591

Table-12: Lift and Drag Co-efficient for Different Frequencies

Cd,F=0	Cl,F=0	Cd,F=.5	Cl,F=.5	Cd,F=1	Cl,F=1	Cd,F=1.5	Cl,F=1.5	Cd,F=2	Cl,F=2
0.362564	0.26	0.215832	0.2	0.310626	0.13	0.352564	0.07	0.352564	0.07
0.324991	0.87	0.362564	0.95	0.29151	0.8	0.279144	0.93	0.279144	0.93
0.283111	1.34	0.299144	1.3	0.282151	1.36	0.210072	1.4	0.210072	1.4
0.199052	1.76	0.211072	1.83	0.20579	1.7	0.189905	2	0.189905	2
0.17159	1.99	0.169905	1.88	0.146451	1.95	0.159014	2.2	0.159014	2.2
0.171794	2.57	0.172159	2.7	0.135597	2.65	0.129718	2.67	0.129718	2.67
0.162286	2.92	0.152718	2.99	0.140056	2.84	0.135623	2.98	0.135623	2.98
0.243931	2.31	0.262286	2.5	0.174921	2.6	0.349309	1	0.349309	1
0.364393	0.2	0.325362	0.32	0.374921	0.81	0.428641	0.2	0.428641	0.2

## APENDIX B

Co-efficient of Pressure,  $C_p = \frac{P - P_\infty}{q_\infty}$

$$C_p = \frac{P - P_\infty}{\frac{1}{2} \rho_\infty U_\infty^2}$$

Co-efficient of Lift,  $C_l = \frac{1}{c} \int_0^c (C_{p_l} - C_{p_u}) dx$

Co-efficient of Drag,  $C_d = \frac{1}{c} \int_0^c (C_{p_l} - C_{p_u}) dy$

Reduced Frequency,  $F = \frac{f_e x_R}{U_\infty}$